Dean Vortex Instabilities for Reducing Concentration Polarization and Fouling and for Developing New Membrane Module Designs

(Agreement No. MRDP-699-505-93)

by

Georges Belfort, PI
and Hanuman Mallubhotla

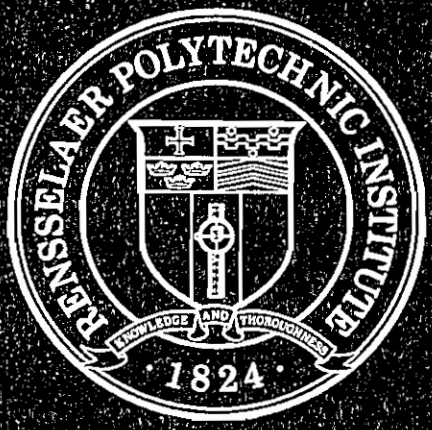

Rensselaer Polytechnic Institute

Troy, New York 12180

Dean Vortex Instabilities for Reducing Concentration Polarization and Fouling and for Developing New Membrane Module Designs

(Agreement No. MRDP-699-505-93)

b y

Georges Belfort, PI
and Hanuman Mallubhotla

Howard P. Isermann Department of Chemical Engineering
Rensselaer Polytechnic Institute
Troy, New York 12180-3590

Dean Vortex Instabilities for Reducing Concentration Polarization and Fouling and for Developing New Membrane Module Designs

(Agreement No. MRDP-699-505-93)

for

National Water Research Institute
105000 Ellis Ave.,
P.O. Box 20865
Fountain Valley, CA 92728-0865

by

Georges Belfort, PI
and Hanuman Mallubhotla

Howard P. Isermann Department of Chemical Engineering
Rensselaer Polytechnic Institute
Troy, New York 12180-3590

April 1994

OUTLINE

SUMMARY

Considerable progress has been made during this six-month project. We have tested the effectiveness of vortex depolarization at higher flow rates around a curve than was previously possible in our laboratory. We increased the Dean number from 3.83 to 6.1, i.e. an 80% increase in the flow rate. In addition, as promised in the proposal, we have formulated a theory for describing solute mass transport and incorporating varying viscosity, diffusivity and osmotic pressure in the three-dimensional convective diffusion equation. Additional experiments have shown the effect of varying transmembrane pressure, styrene/divinyl benzene (S/DVB) particle concentration, and ionic strength on performance. Also, we have evaluated the permeation flux as a function of decreasing and increasing cross-flow rate. To help explain these results, we have developed our own theory and used theories of others especially with respect to colloidal destabilization.

The overall picture we now have is that Dean vortices can indeed make a substantial difference on the performance of pressure-driven membrane filtration processes. The real potential has yet to be tapped.

1.0 INTRODUCTION

During the past few years several researchers have shown that fluid instabilities can effectively depolarize and clean membranes that experience concentration polarization and fouling [see review in 1]. This has been accomplished with inserts in the flow channel [2,3], using flow pulsations of the feed flow [4,5], and with rough membrane surfaces [6,7]. Apparently, the formation of well-controlled instabilities allows more efficient use of the vortices and lower energy losses. These types of instabilities have recently been incorporated into commercial module designs by rotating an inner cylinder within a stationary outer cylinder [8,9], by rocking the module on a torsion spring [10], and by rotating a disc above a flat sheet membrane [11,12]. In an effort to overcome some of the flaws associated with these designs, Belfort et al. have conceptualized a new module design that forms well-controlled centrifugal Dean instabilities[13,14-17]. The work reported here follows our earlier effort and has the goal of demonstrating that such Dean vortices emanating from sufficient flow around a curved channel will indeed result in higher permeation fluxes than crossflow in a flat channel without Dean vortices.

The specific aims for this six-month research project are to (i) test the effectiveness of vortex depolarization at higher flow rates around a curve than was previously possible, and (ii) to formulate a theory for describing solute mass transport and incorporating varying viscosity, diffusivity and osmotic pressure in the three-dimensional convective diffusion equation. In addition, we will also present results that show the effect of varying transmembrane pressure, particle concentration, and ionic strength on performance. After presenting some theory to help explain the results, the materials and methods used in the experiments are reviewed. The results are then presented and discussed in light of previous work and the theory.

2.0 THEORY

2.1 Pressure and flow rate effects - the resistance model

Using the phenomenological approach [18,19], the simple resistance model is given by

$$J \equiv \frac{1}{A}\frac{dV}{dt} = \frac{\Delta p}{\eta_o(R_m+R_c)} , \qquad (1)$$

where J is the permeate flux, V is the total volume of permeate, A is the external membrane surface area, t is the filtration time, Δp is the pressure drop imposed across the cake and membrane, η_o is the viscosity of the permeate, R_m is the membrane resistance, and R_c is the cake resistance. R_m is obtained from the pure water run, since R_c can be neglected and J and η_o are measured.

For a flat membrane design as in our case, the resistance for an incompressible cake is proportional to the cake thickness, δ_c:

$$R_c = \hat{R}_c \delta_c . \qquad (2)$$

where $\hat{R}_c$ is given by the Carman-Kozeny equation [20]:

$$\hat{R}_c = K'(1-\varepsilon_c)^2 S_c^2/\varepsilon_c^3 , \qquad (3)$$

where ε_c is the void fraction of the cake and S_c is the solids surface area per unit volume of solids in the cake. For rigid spherical particles of radius a, the specific surface area is $S_c=3/a$, the void fraction of a randomly packed cake is $\varepsilon_c \approx 0.4$, and the constant K' is approximately 5.0 [21]. It is often convenient to define

$$R_c' = \hat{R}_c/(\rho_s \phi_c), \qquad (4)$$

where ρ_s is the mass density of the solids comprising the cake, $\phi_c = 1 - \varepsilon_c$ is the solids volume fraction of the cake, and R_c' is the cake resistance per unit mass deposited per unit surface area.

Many cake materials, such as the suspended S/DVB particles with extended tentacles of charged emulsifier, are compressible, exhibiting a decrease in void volume and an increase in the specific resistance as the differential pressure is increased. The effects of cake compressibility are often estimated by assuming that the specific cake resistance is a power-law function of the imposed pressure drop [18,22]:

$$R_c' = \alpha_o(\Delta p)^s , \qquad (5)$$

where α_o is a constant related primarily to the size and shape of the particles forming the cake, and s is the cake compressibility which varies from zero for an incompressible cake to a value near unity for a highly compressible cake. These quantities are determined by measuring the specific cake resistance at various pressure drops and then plotting the logarithm of R_c' versus the logarithm of Δp.

Another mechanism could increase the specific resistance by effecting the void volume through an increase in the ionic strength of the suspension causing a compression of the cake. This is discussed below.

2.2 Particle concentration effects

The presence of suspended colloids and particles will affect the flow properties, causing the viscosity of a suspension (η) to differ from that of the pure fluid (η_O, water in our case). Hiemenz [23] gives the following expression for the viscosity of a suspension with a volume fraction of solids of Φ,

$$\eta/\eta_O = 1 + 2.5\Phi + k_1\Phi^2. \qquad (6)$$

where $\Phi < 0.40$ and k_1 has a value of about 10 for spheres. As $\Phi \rightarrow 0$, this result reduces to the Einstein linear equation for dilute suspensions ($\Phi < 0.10$) where $\eta/\eta_O = 1 + 2.5\Phi$. Note that these expressions are independent of particle size.

2.3 Ionic strength effects

Most suspended colloids and particles in nature are negatively charged. The size, size distribution (see discussion below) and the charge of suspended material are crucial to their propensity to foul microfiltration membranes. It is important to realize that flocculation of colloidal material and hence its stability can be strongly influenced by transport processes (diffusion and/or convection), ionic strength of the solution in which the colloids are suspended, the concentration of the colloids or particles, and the intermolecular forces between the suspended particles and between the particles and the membranes.

Consider two identical spherical particles of radius "a" and wall potential Ψ_W interacting through a distance $h_O < a$, in an aqueous solution of a non-adsorbing indifferent electrolyte. For large Ψ_W (>240 mV), one obtains the total interaction potential V on adding the repulsive and attractive potentials [24],

$$V = V_r + V_a = 2\pi a\varepsilon[4RT\gamma/(zF)]^2\exp(-h_O/\kappa^{-1}) - aA/(12h_O). \qquad (7)$$

where $\gamma = \tanh[zF\Psi_W/(4RT)] \approx 1.0$ for large wall potential Ψ_W, and the Debye length $\kappa^{-1} = [2000e^2N_AI/\varepsilon kT]^{-1/2}$, $I = 0.5\Sigma z_i^2M_i$ is the ionic strength, $\varepsilon = \varepsilon_r\varepsilon_O = 78.54\text{x}8.85\text{x}10^{-12}$ (C^2/J-m), $k = 1.38\text{x}10^{-23}$ (J/K), $e = 1.60\text{x}10^{-19}$ (C) and $N_A = 6.02\text{x}10^{23}$ (molecules/mol). At 25°C, $\kappa^{-1} = 4.31\text{x}10^{-10}(2I)^{-1/2}$ (m). For rapidly flocculating colloids, $V \leq 0$, while for a stabilized system, $V > 0$. In the latter case, one obtains the distance of the primary maximum total interaction potential by differentiating **Eq.** (7) and setting it to zero, and then finding that $h_O,max = \kappa^{-1}$(critical). Inserting this result into **Eq.** (7) gives,

$$\kappa^{-1}(\text{critical}) \approx Az_i^2/\gamma^2 \quad (8)$$

and from the definition of the Debye length, $\kappa^{-1} \approx (z_i^2 M_i)^{-1/2}$, where M_i is the molar concentration of ions. Combining this with **Eq. (8)** we obtain the criterion for the critical flocculating electrolyte molar concentration,

$$M_{i(\text{critical})} \approx \gamma^4/(A^2 z_i^6) \quad (9)$$

with the proportionality coefficient of 3.38×10^{-36} $J^2 mol/m^3$ at 25°C, M_i in mol/m^3 and the Hamaker coefficient A in J. **Eqs. (8)** and **(9)** are only valid (in their current forms) for symmetric electrolytes (1:1, 2:2, or 3:3, but not 1:2, etc). For large Ψ_w (>240 mV), $\gamma \approx 1.0$, **Eq. (9)** predicts that the critical flocculating concentration of indifferent electrolytes such as K^+, Ca^{2+} & Al^{3+}, containing counter ions with charge numbers z = 1, 2 & 3 will be in the ratio of $1:2^{-6}:3^{-6}$ or 1000:15.6:1.37 (called the Schulze-Hardy Rule). The above analysis is known as the DLVO theory after Derjaguin, Landau, Verwey and Overbeek [**25**].

2.4 Reversibility effects

2.4.1 Centrifugal instabilities

We have previously shown that for centrifugal instabilities, the driving force across a membrane is given by the mean measured transmembrane pressure minus the centrifugal force which is proportional for flow rate around a curve squared [**26,27**]. This flow rate is expressed as an azimuthal Reynolds number called Dean number, where $De = (2dV/\nu)\sqrt{2d/r_c}$, where d is the half channel height, V is axial mean velocity, ν is the kinematic viscosity and r_c is the centerline radius of the curved channel. The critical De_c is a funtion of curvature or radius ratio R_1/R_2. For our system $De_c = 35.71$. Also, we define $De/De_c \equiv D$.

2.4.2 Governing equations for fluid flow

In terms of the pressure p, kinematic viscosity ν, density ρ and velocity function **v**, the Navier-Stokes equations describe the fluid flow as

$$\nabla \cdot \mathbf{v} = 0 \quad (10)$$

$$\mathbf{v} \cdot \nabla \mathbf{v} = -\rho^{-1} \nabla p + \nu \nabla^2 \mathbf{v} \,. \quad (11)$$

Expressing the vector differential operators in terms of cylindrical coordinates (r,θ and z), the usual boundary conditions for the velocity component v_θ applies: this tangential velocity vanishes on the outer wall at radius R_2 and at the inner wall at radius R_1. For the radial velocity v_r, we take this normal component to be zero at the outer (impermeable) wall and proportional to the pressure difference across the porous membrane at the inner wall. In our design we have placed the membrane test cell on the inner wall.

We approximate the flow as having a weakly coupled θ-component. Specifically, we take the azimuthal flow to be that arising from a weak, constant pressure gradient when both inner and outer boundaries are impermeable. This idealized flow, which depends only on the radial coordinate, then feeds a small radial flow that describes the flow through the membrane of the inner boundary. In this approximation, there then exists an angle-independent solution to Eq. (11) for the radial component of the flow. Since the two velocity components and the pressure gradient vary only with radius r, the governing equations for v_r, v_θ and pressure p become

$$v_r \frac{dv_r}{dr} - r^{-1} v_\theta^2 = -\rho^{-1} \frac{dp}{dr} + \nu \left(\frac{d^2 v_r}{dr^2} + r^{-1} \frac{dv_r}{dr} - r^{-2} v_r \right) \tag{12}$$

$$v_r \frac{dv_\theta}{dr} + r^{-1} v_r v_\theta = -\rho^{-1} r^{-1} \frac{dp}{d\theta} + \nu \left(\frac{d^2 v_\theta}{dr^2} + r^{-1} \frac{dv_\theta}{dr} - r^{-2} v_\theta \right) \tag{13}$$

$$\frac{d(r v_r)}{dr} = - \frac{\partial v_z}{\partial z} \tag{14}$$

Assuming v_r is small, the momentum equation in the r-direction from Eq (12) becomes

$$\frac{dp_r}{dr} = \frac{\rho}{r} v_\theta^2 \tag{15}$$

Now, we replace the partial derivative on the right-hand side of Eq. (14) by a function proportional to the idealized axial flow (which is the solution to Eq (13) with v_r very small)

$$v_\theta(r) = \frac{\partial p_{tc}/\partial \theta}{2\eta_o} \left(r \ln r + Cr + E/r \right) \tag{16}$$

where $\partial p_{tc}/\partial\theta$ is the axial pressure drop in the flow direction θ. The constants C and E are given by [28,29]:

$$C = \frac{R_1^2 \ln R_1 - R_2^2 \ln R_2}{R_2^2 - R_1^2} \quad \text{and} \quad E = - \frac{R_1^2 R_2^2 \ln(R_1/R_2)}{R_2^2 - R_1^2} \tag{17,18}$$

Substituting $v_\theta(r)$ from Eq (16) into Eq. (15) above and integrating from $r = R_1$ to $r = R_2$ gives

$$p(R_2) = p(R_1) - \frac{1}{4(R_1^2 - R_2^2)^2}$$

$$\Big(-12R_1^2R_2^4 ln R_1 \left(ln R_2\right)^2 - 12R_1^4R_2^2 ln R_1 \left(ln R_2\right)^2 + 4R_1^4R_2^4 ln R_2 \left(ln R_2\right)^3$$

$$+ 12R_1^4R_2^2 ln R_2 \left(ln R_1\right)^2 + 4R_2^4R_1^2 \left(ln R_2\right)^3 - 3R_1^4R_2^2 + 3R_1^2R_2^4 - R_2^6$$

$$- 4R_1^2 \left(ln R_1\right)^3 R_2^4 + R_1^6 - 4R_1^4R_2^2 \left(ln R_1\right)^3 + 12R_1^2R_2^4 ln R_2 \left(ln R_1\right)^2 \Big) \qquad (19)$$

We now wish to simplify the expression above in the limit that the gap size is small. Thus, we define a dimensionless parameter $\varepsilon = (R_2 - R_1)/R_1$. This means $R_2 = R_1 (1 + \varepsilon)$. We need to replace R_2 in the equation above for $p(R_2)$ in terms of ε. The term in large brackets has a non-zero leading order term proportional to ε^7. The lower orders cancel. The denominator of the coefficient multiplying the large brackets goes as ε^2. Thus, the lowest order approximation is linear in ε^5 and looks like

$$p(R_2) = p(R_1) + \rho \cdot \frac{\left(\partial p_{\tau c}/\partial \theta\right)^2}{16\eta_o^2} R_1^2 \left(\frac{2}{15}\varepsilon^5\right) \qquad (20)$$

2.4.3. A test example

For the present system, $R_1 = 61.9 \times 10^{-3}$ m and $\varepsilon = 0.02585$. Using $\eta_o = 10^{-3}$ kg/m-s and $\rho = 10^3$ kg/m^3, we obtain from Eq. (**20**)

$$p(R_2) = p(R_1) + 3.684 \times 10^{-4} \left(\frac{\partial p_{\tau c}}{\partial \theta}\right)^2 \qquad (21)$$

For D = 6.1, Q = 6.21 *l*/min, De = 217.8. (The abscissa in **Fig. 16** from Kuelagan and Beij, (**34**) is 154.03). The ratio of pressure loss in a curved channel to that in a straight channel is $(\lambda_c/\lambda_s) \approx 1.7$. The pressure loss in a straight channel is given by the Hagen-Poisuelle equation,

$$\Delta P = \frac{8\eta_o \, l \, Q}{\pi(2d)^4} \qquad (22)$$

Substituting for $l = \frac{(R_1 + R_2)}{2}\theta = (62.7 \times 10^{-3})\theta$, (in m) into Eq. (**22**),

$$\left(\frac{\Delta P}{\theta}\right)_{straight} = 2521 \frac{kg}{m\text{-}s^2} \quad (23)$$

For the curved channel, then

$$\left(\frac{\Delta P}{\theta}\right)_{curved} = 1.7\ (2521) = 4286.64 \frac{kg}{m\text{-}s^2} \quad (24)$$

$$p(R_2) = p(R_1) + 6769.45 \quad (25a)$$

where all the terms are in kg/m-s^2. Or,

$$p(R_2) = p(R_1) + 6.68 \quad (25b)$$

where the pressures are expressed in kPa.

For the present system, however, the axial pressure drop has been measured by Chung, et al. (15). This was 0.0475 psi/in, which is equivalent to 1289.63 kg/m^2-s^2. The length of the membrane is 76.2 mm, giving,

$$\left(\frac{\Delta P}{\theta}\right)_{actual} = 12893.63 \times 76.2 \times 10^{-3} = 982.495 \text{ kg/m-s}^2$$

Substituting for $(\partial p_{\tau c}/\partial\theta)$ in the pressure equation

$$p(R_2) = p(R_1) + 0.351 \quad (26)$$

in units of kPa. The additional term on the right hand side of the equation is less than the experimental error. The centrifugal force is expected to diminish the transmembrane pressure and hence the pure water flux. However, the effect is negligible for this system validating the observations of Chung, et al. (**15**) that the water flux does not change with the presence of Dean vortices. This is due to the decay of the Dean vortices with axial distance by the time they reach the membrane surface (see discussions in (**15**) and (**26**).

2.4.4 Variable properties

The velocity components v_r, v_θ and v_z and the pressure gradient in the θ-direction are first obtained from a solution to the the Navier-Stokes equations [Eqs (**12-14**)] with the appropriate boundary conditions. Then they are substituted into the convective diffusion equation:

$$\frac{\partial uc}{\partial r} + \frac{1}{r}\frac{\partial vc}{\partial \theta} = D\left(\frac{1}{r}\frac{\partial}{\partial r}\left(r\frac{\partial c}{\partial r}\right)\right) + \frac{1}{r^2}\frac{\partial c}{\partial \theta} + \frac{\partial^2 c}{\partial \theta^2} \quad (27)$$

Expressions for variable viscosity, η are given by Eq (5). The variable diffusivity and osmotic pressure can be obtained from the equations listed below.

Osmotic pressure: An aqueous feed solution, as defined here, is one in which the solutes are completely dissolved. Salts and small organic molecules such as sugars, small peptides, amino acids, urea, alcohols etc. are characterized by very high osmotic pressures and mutual diffusion coefficients. For an ideal (dilute) solution, the osmotic pressure (in KPa) can be estimated by van't Hoff's equation,

$$\Pi = vcRT/M \tag{28}$$

where v is the number of ions formed if the solute dissociates, c is the solute concentration in kg/m^3, R = 8.314×10^3 kg-$m^2/(s^2$-°K-kg-mol), T is the temperature in °K, and M is the molecular weight in kg/kg-mol. For small molecules such as sucrose (M = 342 kg/kg-mol) at c = 50 kg/m^3 and 20°C, Π = 0.356 MPa. For large colloids (M = 10^7 kg/kg-mol) at the same concentration and temperature, Π = 1.22×10^{-5} MPa. Intermediate size solutes such as proteins can also exert relativley high osmotic pressures when present at large concentrations. The buildup of large colloids and particles, on the other hand, exert negligible osmotic effects.

Diffusivity: A colloidal suspension, as defined here, is one in which particles with a linear dimension of between 10^{-9}-10^{-6} m (nanometers to micrometers) are suspended in an aqueous fluid [23]. Particles much larger than a micrometer in linear dimension are considered large particles with respect to MF. The range of particle sizes of most interest for MF is 0.1-20 μm and is relevant for several industrial fluids. For colloidal particles where M is very large, Π is negligible as compared to the transmembrane pressure for microfiltration (Δp = 100-300 KPa). The translational diffusion coefficient of suspended colloids and particles (in units m^2/s) can be estimated at *infinite dilution* from the Einstein-Sutherland equation,

$$D_o = kT/f \tag{29}$$

where k is Boltzmann's constant (=1.380×10^{-23} J/molecule-°K) and f is the frictional coefficient (kg/s-molecule). For hydrated flexible macromolecules, obtaining an estimate of f is difficult (see Cantor and Schimmel [30]). However, for rigid colloidal particles of dimension much larger than the hydrated layer, f can be obtained from the classical Stokes law and the Perrin shape factor, F,

$$f = 6\pi\eta aF \tag{30}$$

and

$$F = f/f_{sph} = (1-p^2)^{1/2}/\{p^{2/3}H\} \tag{31}$$

where for a prolate ellipsoid with p = b/c, $H = \ln\{[1+(1-p^2)^{1/2}]/p\}$, and for an oblate ellipsoid with p = c/b, $H = \tan^{-1}[(p^2-1)^{1/2}]$, and where c/b is the ratio of the long to the short semiaxes. F has been both plotted and tabulated as a function of p by

Cantor and Schimmel [30]. For a sphere, F = 1. η is the viscosity (Pa-s) and a is the radius (m) of an equivalent sphere with the same volume as the non-spherical solute. The volumes of the three shapes are $(4/3)\pi a^3$ (sphere), $(4/3)\pi c^2 b$ (oblate), and $(4/3)\pi c b^2$ (prolate).

From Eq (29) D_O is proportional to T/f and from Eq (30) f is proportional to η, therefore $D_O \propto T/\eta$ or

$$D_O/D_S = T\eta_S/(T_S\eta) \qquad (32)$$

where D_O & D_S and η & η_S are the solute diffusion coefficients and the viscosities of the fluid at the temperatures T and T_S (standard), respectively. Using Eqs (29) & (30) for a suspended sphere in a fluid with the viscosity of water (1 cp) at 20 °C, $D_O = 2.15 \times 10^{-19}/a$ (with D_O in m^2/s and a in m). Hence for a micron size sphere in water, $D_O = 2.15 \times 10^{-13}$ m^2/s, some three to four orders of magnitude lower than the diffusivity of glycine or sodium chloride! As will be seen below, this has a significant effect on the Brownian back-diffusion of colloids away from the membrane and on the potential of large colloids and particles to foul MF membranes. Others have used an empirical expression.

$$\frac{D}{D_O} = \exp(b\phi), \qquad (33)$$

to describe the diffusivity as a function of solids volume fraction, ϕ.

3.0 MATERIALS AND METHODS

The flow system has been described in detail by Chung et al. [15]. It consisted of a 180° narrow gap curved slit channel (CSC) with a pump, pulse dampener and rotameter to measure flow rates. A manometer was used to ensure the same transmembrane pressure drop for runs with and without Dean vortices. Different materials and methods were used in this study, however, and these are described below.

3.1 Materials

Membranes: Because of pressure limitations in the CSC and time limitations to obtain a noticeable change in the permeate fluxes, high flux polysulfone (PSf, GRM0.2PP, Dow Danske, Nakskov, Denmark) and polypropylene (PP, Accurel Polypropylene Membranes, AKZO, Enka America Inc., Asheville, NC) microfiltration membranes were used. The nominal pore sizes of both kinds of membranes were 0.2 µm. The drain channel or porous support for the membrane consisted of two sheets of simplex knit fabric (polyester fiber) stiffened with epoxy coating (FilmTec Corp., Minneapolis, MN).

Feed suspensions: The feed suspensions included DI water as a control and polydispersed polystyrene particles. The DI water was prepared by passing Troy city tap water through a reverse osmosis module (FT30, FilmTec Co., Minneapolis, MN), a

mixed strong ion exchange bed, and a UV unit. This gave essentially organic and particle free 19 megohm water. Polydispersed S/DVB particles with a volume medium nominal diameter of 19.2 μm and a density of 1052 kg/m^3, prepared by suspension polymerization of styrene-divinyl-benzene (S/DVB, Dow Chemical Co., Midland, MI), were used at various suspension concentrations (0.0133 to 0.5 wt %) in DI water. The actual particle size distribution is shown in **Fig. 1**, where it can be clearly seen that there are three peaks at about 16.4, 33 & 49 μm, suggesting that the suspension consisted of monomers, dimers and trimers. The particles were dispersed in DI water by magnetic mixing for about 40 minutes, before running the suspension through the system.

Pure KCl, an indifferent electrolyte, was added to the suspensions for the variation of ionic strength experiments.

3.2 Methods

Cleaning: The membranes were cleaned after each experiment until the pure water permeability was regained. First a 0.1 N HNO_3 solution was pumped through the system for about 20 min., then a 0.1 N NaOH was flushed through the system for about 20 min. The system was then exposed to DI water for about 10 min. The water was discarded and fresh DI water was passed through the system for about 30 min. The water permeability was measured at the end of this 30 min period and compared to previously measured values. Back flushing was not possible because of sealing requirements.

Operating Procedures

Flow system: DI water was pumped (either during cleaning or before the start of an experiment) through the system at the same pressures and flow rates at which the particle suspension would later be pumped, to ascertain the valve positions required for the experiment. The pump was then stopped, the tubing switched to the suspension feed tank, and restarted. The required pressures and flow rates were achieved within 2 minutes, with minor readjustments of the valves. A stop watch was started with the first drop of permeate obtained and permeate flow was measured with time. The system achieved pseudo-steady state in about an hour (**Fig. 2**). However, the permeate flux value obtained at about 30 minutes was within 5 % of the final permeate flux value. In order to save time, the value at 30 min was used for subsequent experimental runs. The membrane was exposed to approximately the same feed solution throughout the experiment. This was possible since real changes in concentration were very small due to the large feed volume (15 l) and small transport area of the membrane (the active surface area of the membrane was 48.4 cm^2). Collected permeate was returned to the feed tank periodically. For any given period, not more than 500 ml of permeate remained in the permeate collector.

After completing the experiment with vortices (flow around the curve and then across the membrane), the membrane was cleaned as described above and while passing the DI water through the system, the valve positions were changed such that the *flow configuration* for the experiment without vortices was established (flow across the membrane and then around the curve).

Conductivity experiments: To investigate the charge effects of the S/DVB particles, conductivity experiments were performed by adding salt to the particle

suspension. Conductivities were measured using a Beckman conductivity meter (Model # 123310, Beckman Instruments Inc., Fullerton, CA). The conductivity meter was calibrated using standard solutions of KCl. The conductivity of particle suspensions (200 to 1000 ml) were then measured while adding known amounts of KCl to the suspensions. The suspensions were equilibrated with the added KCl by stirring for about 10 min before measuring the conductivity.

To investigate particle shielding effects, about 1000 ml of the particle suspensions were prepared (at three particle concentrations) and separated into 10 samples of 100 ml each. Different amounts of KCl were added to the samples and conductivities were measured. The suspension samples were then placed in metal centrifuge-sheaths and centrifuged (5000 to 10000 rpm, 4 min) to separate the latex particles from the supernatant. Because the presence of metal affected the measured conductivity, the supernatants were decanted into glass beakers before measuring the conductivity.

4.0 RESULTS AND DISCUSSION

4.1 Results

In earlier work, we mainly varied the flow rate around the curved channel [**15**]. Below, we present results that show the effects of changing the transmembrane pressure, the suspended solids concentration, the ionic strength of the solution, and we extend the range of the flow rate from a maximum earlier value of $De/De_c = D =$ 3.8 to 6.1.

4.1.1 Pressure Effects

Using a convenient and standard way of determining pressure effects on performance, the permeation flux is plotted against the transmembrane pressure (ΔP) in **Figs. 3 & 4** for 0.2 μm nominal pore size PSf and PP membranes, respectively. The flux improvement for the PSf membrane varied from 15 % at 100 KPa to 30 % at 70 KPa, and for the PP membrane varied from 39 % at 35 KPa to 43 % at 73 KPa. For the latter case, the improvement with vortices increased with increasing transmembrane pressure. These flux improvements were obtained at D=4.8 and 6.1 and at latex concentrations of 0.15 and 0.075 wt %, respectively, as compared to an improvement of about 15 % obtained previously at D=3.8 and 0.1 wt % [**15**]. The differences were probably due to the different mean particle size and dispersity of the suspended particles. In **Fig. 5**, the suspension flow rate was varied in order to determine the upper limit of the flux improvements by increasing the intensity of Dean vortices (i.e. the D values). The rate of flux improvements decreased with increasing transmembrane pressure, except for the slowest flow rate case. At 73 KPa and D=6.1, an improvement of about 43 % was observed.

The significance of these results is that Dean vortices improved performance, this improvement was effective at all transmembrane pressures studied, and the largest improvements were observed at the highest transmembane pressures and fastest flow rates.

4.1.2 Particle concentration effects

We next wanted to determine the permeation flux improvement as a function of solids concentration in the feed suspension, C_b. Clearly, as the feed particle concentration diminishes to small values, the potential to form a concentration polarization and/or a fouling layer at the membrane-solution interface is reduced, and the advantage of having Dean vortices becomes negligible. On the other hand, at very high particle concentrations, the effectiveness of the Dean vortices in depolarizing or defouling the membrane is also reduced due to increased viscosity and particle-particle interactions. The result of these effects are shown in **Fig. 6** for a D= 4.77 and ΔP=69.8 KPa and a 0.2 μm PSf membrane. The effect of particle concentration with changing ΔP is shown in **Fig. 7.** In both cases (0.075 and 0.133 wt %), the improvement with Dean vortices increases with ΔP with larger fluxes and a larger increase seen with the lower particle concentration. Plotting the flux versus logarithm of the bulk solids concentration in **Fig. 8a & b** for S/DVB and silica suspensions, we see that Dean vortices do indeed give higher fluxes.

Clearly, as the solids weight fraction increases during concentration with microfiltration, it becomes imperative to increase the intensity of the vortices, i.e. flow at a faster rate.

4.1.3 Ionic strength effects

It is important to know whether Dean vortices can improve the performance during microfiltation of a S/DVB particle suspension with changing ionic strength. This is shown in **Fig. 9** for D=6.1 at ΔP=35 KPa and with a 0.2 μm PP membrane at two different concentrations (**Fig. 9a**: 0.133 & **Fig. 9b**: 0.2 wt %). As the ionic strength (KCl concentration) increased, the permeation flux first decreased and then increased to a constant value. The improvement with vortices remained steady at about 32 and 24 % throughout the range of ionic strength for the 0.133 and the 0.2 wt % particle concentrations, respectively. Thus, addition of salt to the suspension had little effect on the flux improvement, rather the particle concentration was again determining.

4.1.4 Reversibility effects

We have shown previously [15] and in **Fig. 5** above that operating from the beginning of a run at a high axial flow rate (D>1) results in strong Dean vortices and hence improved performance over that without such vortices (i.e. when D<1). However, previous work has suggested that these effects may not be reversible. To test this, we performed a series of measurements in which the axial flow rate (D) was cycled from a high value to a low value close to 1 and back up again. A micro-filtration membrane (0.2 μm PP) was used to filter a 0.07-0.075 and a 0.2 wt % S/DVB particle suspension at ΔP=35 KPa in separate experiments. The results, summarized in **Fig. 10**, demonstrate the irreversible behavior of the flow rate (D values) on permeation flux, J. As D is decreased from a high value of 6.1 to 3.3 (A-B in **Fig. 10a**) or to below 1 (A-B in **Fig. 10b**), the *expected* drop in performance is observed. However, as D is increased from these low values back up to the original high values (B-C in **Fig. 10**), an *unexpected* drop in performance is observed. Reducing the flow rate once again, results in a further decrease in performance but apparently reaches a minimum plateau (from C-D-E in **Fig. 10b**). By thoroughly scrubbing the membrane, the permeation flux at point A can be restored from that at point E in **Fig. 10b**.

These results suggest that if operated at high flow rates, Dean vortices were able to reduce polarization and fouling but that once these unwanted effects occurred, the relatively weak Dean vortices tested here were not only unable to recover performance but actually resulted in a *lowering* of performance.

4.2 Discussion

In order to understand the results presented here, it is necessary to focus on the behavior of the disperse colloidal suspension used in this study. Referring to the literature and the current understanding of the behavior of colloid stability, we will attempt to explain the observations noted above.

4.2.1 Pressure Effects

The change-over from a vortex-free to a vortex-containing fluid during flow around a curve is due to an increasing centrifugal force from an increasing axial flow rate. This induces a Dean vortex instability. From Dean's original analysis and from our recent work on curved porous walled slit channels [28], the curved flow Reynolds number (called the Dean number, De) can be used to indicate the existence and strength of the Dean vortices. From Eq (15) it is evident that the pressure drop in the r-direction is proportional to v_θ^2 or De^2 or D^2. Since the permeation flux is proportional to the pressure drop across the membrane ($\frac{dp_r}{dr}$), called the transmembrane pressure drop with distance, Δp_{tm}/thickness of the membrane). Thus, the flux improvement, ΔJ is plotted against against D^2, where D is the ratio of the De to De_C (=35.71) and $\Delta J = J_V - J_O$, i.e., the permeation flux obtained in the presence minus that obtained in the absence of vortices. Linear plots at different transmembrane pressures, ΔP, with a converging point at $D^2 = D = 1.0$ is observed in **Figs. 11 & 12** for S/DVB particle and silica suspensions at different concentrations. In most cases the plots appear to converge to D = 1.0, as expected. As the concentration of the suspensions increased, the percent flux improvement declined as expected. At a given flow rate (Dean number ratio, D), the flux improvement increased with increasing transmembrane pressure. This independently confirms the results shown in **Fig. 5.**

4.2.2 Particle concentration effects

Apparently, a flow rate of D = 4.77 was insufficient to maintain an improved flux when the particle concentration increased above about 0.2 wt % as shown in **Fig. 6a.** Assuming that the S/DVB particle concentration at the membrane-suspension interface is given by the following polarization model for the length-averaged permeate flux [31]:

$$\langle J \rangle = 0.81 \left(\dot{\gamma}_o D_{Bo}^2/L\right)^{1/3} \ln(\phi_w/\phi_b) = 0.114 \left(\dot{\gamma}_o k^2 T^2/\eta_o^2\, a^2 L\right)^{1/3} \ln(\phi_w/\phi_b) \quad (34)$$

where $\dot{\gamma}_o$ wall shear rate, D_{Bo} is the difusivity, L is path length, ϕ_w and ϕ_b are the volume fraction of solids at the membrane surface and in the bulk suspension, respectively. For both S/DVB and silica suspensions in **Fig. 8**, Eq (34) holds only for part of the concentration range (linear trends). The fluxes were higher with than

without vortices. The slopes in the linear region were similar for the silica case. The flux advantage with vortices becomes more noticeable as the bulk concentration is reduced.

Since the predicted flux for the Brownian diffusion mechanism increases with shear rate or feed velocity to the one-third power, and decreases with particle radius to the two-thirds power. The particle volume fraction, ϕ_w, in the boundary layer immediately above the thin fouling layer on the membrane surface may be determined experimentally from a semi-log plot of flux versus bulk particle concentration. Alternatively, if the particles are non adhesive, then ϕ_w will be equal to the maximum random packing density of particles in the adjacent cake layer, and it may then be estimated that $\phi_w \approx 0.6$ for rigid spherical particles of equal size and $\phi_w \approx 0.8$-0.9 for compressible or polydisperse particles. Rearranging Eq. (34) for the wall solids concentration

$$\left(\frac{\phi_w}{\phi_b}\right) = \exp\left(\frac{< J>}{0.81}\left(\frac{L}{\dot{\gamma}D^2}\right)^{1/3}\right). \qquad (35)$$

An estimate of the expression in the large bracket on the RHS of Eq (35) for the data in **Fig. 2** ($<J>=10^{-3}$ cm/s, L=10, $\dot{\gamma}=2500$ s^{-1}, and $D=10^{-9}$ cm^2/s) is 195. Thus, the concentration and hence the viscosity near the wall will be very much larger than in the bulk suspension away from the wall.

4.2.3 Ionic strength effects

The double layer thickness for a 0.1 M KCl solution (middle of the range in **Fig. 9**) is $\kappa^{-1} = 0.304/I^{1/2} = 0.96$ nm, while an estimate of the size of the spatial extension of the adsorbed sodium lauryl sulfate (SDS, M=288.4 Da) is given by the r.m.s. end-to-end length as [25]

$$< r^2 >^{1/2} = 0.06\ M^{1/2} \qquad (36)$$

and equals 1.02 nm. Thus, the anionic detergent extends into the solution about one nm. If, when exposed to large salt concentrations, the repulsive forces on the anionic detergent are reduced. The detergent will then be able to aggregate with similar molecules on other particles and/or fold onto itself. Dimers and trimers will result from this flocculation process (**Fig. 1**). The thickness of these layers are relatively very small as compared to the diameter of the suspended S/DVB particles (monomer diameter 16 μm).

The following arguments are preliminary and somewhat speculative since we do not as yet have enough data to support these arguments. In order to explain the behavior of the flux with increasing ionic strength ([KCl]) as seen in **Fig. 9**, two competing phenomena need to be considered. First, one needs to consider the flocculation of colloidal particles (see above) due to addition of salt causing the emulsifier molecules (tentacle-like flocculant molecules attached to the surface of the S/DVB particles) to bridge between colloids. This results in a flux *increase* with salt addition, since larger colloids (i) can be inertially *lifted away* from the cake more effectively than smaller colloids (proportional to a^3 [32]), and (ii) form *more porous*

cakes (proportional to a^2). For the three particle sizes (16.4, 33 & 49 μm) seen in **Fig. 1**, the ratios for an increased flux for a^2 are 1:4:9 and for a^3 are 1:8:27.

On the other hand, as salt is added the colloids in the cake also experience less steric repulsion and hence densify with salt addition. This causes a *decrease* in the flux with salt addition. There reaches a point at which the colloids cannot get any closer (proportional to the bulk colloid concentration and hence the cake concentration as seen in **Fig. 13**) as the emulsifier molecules are coiled to a maximum. Note that in **Fig. 13**, the salt concentration at (i) the minimum is proportional to the particle concentration in the bulk solution, and (ii) the beginning of the flux asymptote is also proportional to the S/DVB particle concentration in the bulk solution! Thus, the ratio of minima (0.075/0.05 in units of mols KCl) is equal to the ratio of the particle concentrations (0.2/0.133 in units of wt % S/DVB), and the ratio at the flux asymptotes (0.15/0.1). A schematic of the competing effects discussed above is shown in **Fig. 14.**

Note that none of these effects are dependent on the presence or absence of vortices and hence the observations are independent of the shear rate. The results are dependent on the *amount* of suspended matter in the bulk solution, suggesting that coagulation is the dominant process both in the suspension and in the cake. Although we still need to confirm that large amounts of emulsifier or soap may slough off the colloid particles and enter the bulk solution, the results strongly suggest that this is indeed happening.

4.2.4 Reversibility effects

In order to understand the flux behavior shown in **Fig. 10**, we need to discuss the formation and structural changes of particulate cakes with time. First, it is important to note that our bulk solution comprises of at least three and likely more particle sizes. The result of having a particle size distribution in the feed are: (i) smaller particles are preferentially deposited than large particles [32], and (ii) cakes comprised of smaller particles pack closer, are more tightly held, and have less free volume (porosity). Thus, these types of cakes are expected to have larger resistance to flow as expressed by **Eq. (3)**. Second, as cakes consisting of large particles grow in thickness, the cross-section for axial flow in the duct is reduced and the mean axial velocity and wall shear rates are likely to increase (depending of the pump type). This will result in (i) increased inertial lift for larger particles at higher flow rates, and (ii) the top-most layers of the cake will be re-entrained into the feed suspension. Third, with mature cakes, finer particles will infiltrate into a preformed cake consisting of larger particles substantially reducing the permeation flux. Fourth, the permeation flow through the cake will drag particles toward the membrane inducing a hydraulic compression effect [33]. This would force the cake particles closer and would "flatten" the anionic detergent tentacle molecules surrounding the particles, making it difficult to break the cake with Dean vortices.

We believe that the observations presented in **Fig.10**, strongly support the effects described above in a qualitative manner. For example, as the flow rate is decreased a larger fraction of bigger particles deposit onto the cake (A-B in Fig. 10a&b) and the cake builds up with increasing resistance to permeation flow. It also compresses due to drag forming a dense compact cake at point B. As the flow rate is once again increased (B-C), larger particles are lifted away and smaller particles are preferentially deposited. The wall shear rates are insufficient to erode the cake and

the smaller particles intrude into the preformed cake *reducing* the flux unexpectedly. The process is repeated once again (C-D in **Fig. 10b**), however, once D is reached, the cake is relatively thick and at its maximum density and thickness. Few small particles can intrude into the cake and it is already densely packed. Hence, increasing the flow rate has no effect on the flux!

To test the role of particulate aggregates, a similar experiment to that shown in **Fig 10** was run, except a large amount of salt was added to the feed. As we have shown above, this should change the size distribution of the particles. The result is shown in **Fig. 15.** From A-B, the flux drops as expected due to cake build-up. In this experiment, the larger particles were less tightly bound and could be removed from the cake as the flow rate was increased (B-G). Two step increases suggest that a critical shear rate was necessary to remove the top layers from the cake and that this occurred in steps (C-D & E-F).

5.0 CONCLUSIONS

Considerable progress has been made during this six-month project. The following conclusions can be made:

1. Our method of producing well-defined vortices, such as the Dean centrifugal vortices, has a beneficial effect of increasing permeation flux. Flux improvements of up to 45% have been observed. This beneficial effect increased with flow rate and transmembrane pressure and decreased with the concentration of the suspended matter.

2. A theoretical analysis was used to successfully plot the flux improvements for flow with vortices versus flow without such vortices against the flow rate squared. Excellent linear plot resulted.

3. Two competing phenomena occurred during the addition of potassium chloride to the feed suspension. Flux increased due to particle aggregation and inertial lift, while flux experienced a decline due to cake densification. The highest fluxes were obtained at the lowest salt concentration.

4. Because of the size distribution of particles in the feed, aggregation effects, and the effects of particle drag within the cake, increasing and decreasing the flow rate showed clear irreversibility.

5. We have formulated a method to solve the convective-diffusion equation with variable properties. This will be numerically solved in our continuation project.

ACKNOWLEDGMENTS

We thank Dr. Charles J. McDonald for advice and for measuring the particle size distribution (**Fig. 1**).

REFERENCES

1 Winzeler, H. B. and Belfort, G., Enhanced performance for pressure-driven membrane processes: The argument for fluid instabilities, *J. Membrane Sci.*, 80, (1993) 35-47.

2 D. G. Thomas and R.B. Gallaher, Turbulence promoters for hyperfiltration tubes, *Membrane Digest* 1 (1), (1972) 71-102.

3 D. A. Colman and W.S. Mitchell, Enhanced mass transfer for membrane processes, *Trans I ChemE.* 69, Part C (1991) 91.

4 T. J. Kennedy, R. L. Merson, and B. J. McCoy, Improving permeation flow by packed reverse osmosis, *Chem. Engr. Sci.* 29, (1974) 1927-1931.

5 H. Bauser, H. Chmiel, N. Stroh, and E. Walitza, Interfacial effects with microfiltration membranes, *J. Memb. Sci.* 11, (1982) 321-332.

6 M. A. Jeffree, J. A. Peakock, I. J. Sobey, B. J. Belhouse, Gel layer limited haemofiltration rates can be increased by Vortex mixing, *Clin. Exp. Dias. Apheresis* 5, (1981) 373-380.

7 M. J. van der Waal and I. G. Racz, Mass transfer in corrugated-plate membrane modules: I. Hyperfiltration experiments, *J. Memb. Sci.* 40, (1989) 243-260.

8 M. Lopez-Leiva PhD Thesis, "Ultrafiltration in a Rotary Annular Filter" Department of Food Engineering, Lund University, Lund, Sweden (1979).

9 J. Lieberherr, PhD. Thesis "Scerfiltration im Ringspalt" ETH, Zurich, Switzerland (1978).

10 B. Culkin, Vibrating shear enhanced processing applied to liquid-solid separations, paper 3B presented at the NAMS'90 Annual Meeting, San Diego, CA, May 28-31 (1991).

11 J. Murkes and C-G Carlsson, Crossflow Filtration, Theory and Practice, J. Wiley and Sons., (1988).

12 M. Lopez-Leiva, Ultrafiltration at low degrees of concentration polarization: Technical possibilities, *Desalination* 35, (1980) 115-128.

13 W. R. Dean,Fluid motion in a curved channel,*Proc.Roy.Soc. A* 121,(1928)402-420.

14 Brewster, M. G., Chung, K-Y, and Belfort, G., Dean vortices with wall flux in a curved channel membrane system: 1. A new approach to membrane module design, *J. Membrane Sci.*, 81, (1993)127-137.

15 Chung, K.-Y., Bates, R., and Belfort, G. (1993), Dean vortices with wall flux in a curved channel membrane system: 4. Effect of vortices on permeation fluxes of suspensions in microporous membrane, J. Membrane Sci., 81, 139-150.

16 Chung, K-Y, Edelstein, W. A., Li, X. and Belfort, G. (1993), Dean vortices in a curved channel membrane system: 5 Three dimensional magnetic resonance imaging and numerical analysis of the velocity field in a curved impermeable tube, AIChE Journal, in press.

17 Chung, K.-Y.,Edelstein,W.A.,& Belfort, G.(1993),Dean vortices with wall flux in a curved channel membrane system.6.Two dimensional magnetic resonance imaging of the velocity field in a curved impermeable slit, J.Memb.Sci.,81,151.

18 G. Belfort and B. Marx, Artificial particulate fouling of hyperfiltration membranes - II analysis and protection from fouling, *Desalin.* 28 (1979) 13-30.

19 R. H. Davis and D. C. Grant, Theory of deadend microfiltration, in Membrane Handbook, (Eds. W.S. Ho and K.K. Sirkar) Van Nostrand Reinhold, New York, NY, (1992) pp. 461-479.

20 P. C. Carman, Fundamental principles of industrial filtration, *Trans. Inst. Chem. Eng.*, 16 (1938) 168-187.

21 H. P. Grace, Resistance and compressibility of filter cakes, *Chem. Eng. Prog.*, 49 (1953) 303-318.
22 Porter, M. C., What, when, and why of membranes--MF, UF and RO, in What the Filter Man Needs to Know About Filtration, (Ed. W. Shoemaker), AIChE Symp. Ser. Vol. 73, No. 171 (1977) pp. 83-103.
23 P. C. Hiemenz, Principles of Colloid and Surface Chemistry, (second edition), pp. 199, Marcel Dekker, Inc., New York (1986).
24 R. F. Probstein,. Physicochemical Hydrodynamics, An Introduction, Butterworths, Boston, (1989).
25 R. J. Hunter, Foundations of Colloid Science, Vol I, Clarendon Press, Oxford(1986).
26 Belfort, G., Pimbley, J. M., Greiner, A., and Chung, K-Y (1993), Diagnosis of membrane fouling using rotating annular filter 1. Cell culture media, J. *Membrane Sci.*, 77, 1-22..
27 Belfort, G., Mikulasek, P., Pimbley, J. M., and Chung, K-Y (1993), Diagnosis of membrane fouling using a rotating annular filter, 2. Dilute particle suspensions of known particle size, J. *Membrane Sci.*, 77, 23-39.
28 Brewster, M. G., Chung, K-Y, and Belfort, G., Dean vortices with wall flux in a curved channel membrane system: 1. A new approach to membrane module design, *J. Membrane Sci.*, 81, (1993)127-137.
29 Dean W.R.(1928)Fluid motion in a curved channel,*Proc.Roy.Soc.A* 121,402- 420.
30 C. R. Cantor and P. R. Schimmel, Biophysical Chemistry. Part II, Techniques for the Study of Biological Structure and Function, pp 562-565; 581-586, W.H. Freeman & Co., San Francisco, CA. (1980).
31 A. L. Zydney and C.K. Colton, A concentration polarization model for the filtrate flux in cross-flow microfiltration of particulate suspensions, *Chem. Eng. Comm.* 47, (1986)1-21.
32 Drew, D. A., Schonberg, J. A., and Belfort, G. (1991), Lateral inertial migration of a small sphere in fast laminar flow through a membrane duct, *Chem. Eng. Sci.* 46, (12) 3219-3224.
33. Pillay, V.L. (1991) "Modelling of turbulent cross-flow microfiltration of particulate suspensions", Doctoral Thesis, Department of Chemical Engineering, U. of Natal, Durban, South Africa.
34. Keulegan, G.H., and Beij, K.H. (1937) Pressure Losses for Fluid Flow in Curved Pipes, *J. Res. N.B.S.*, 18, 89-114.

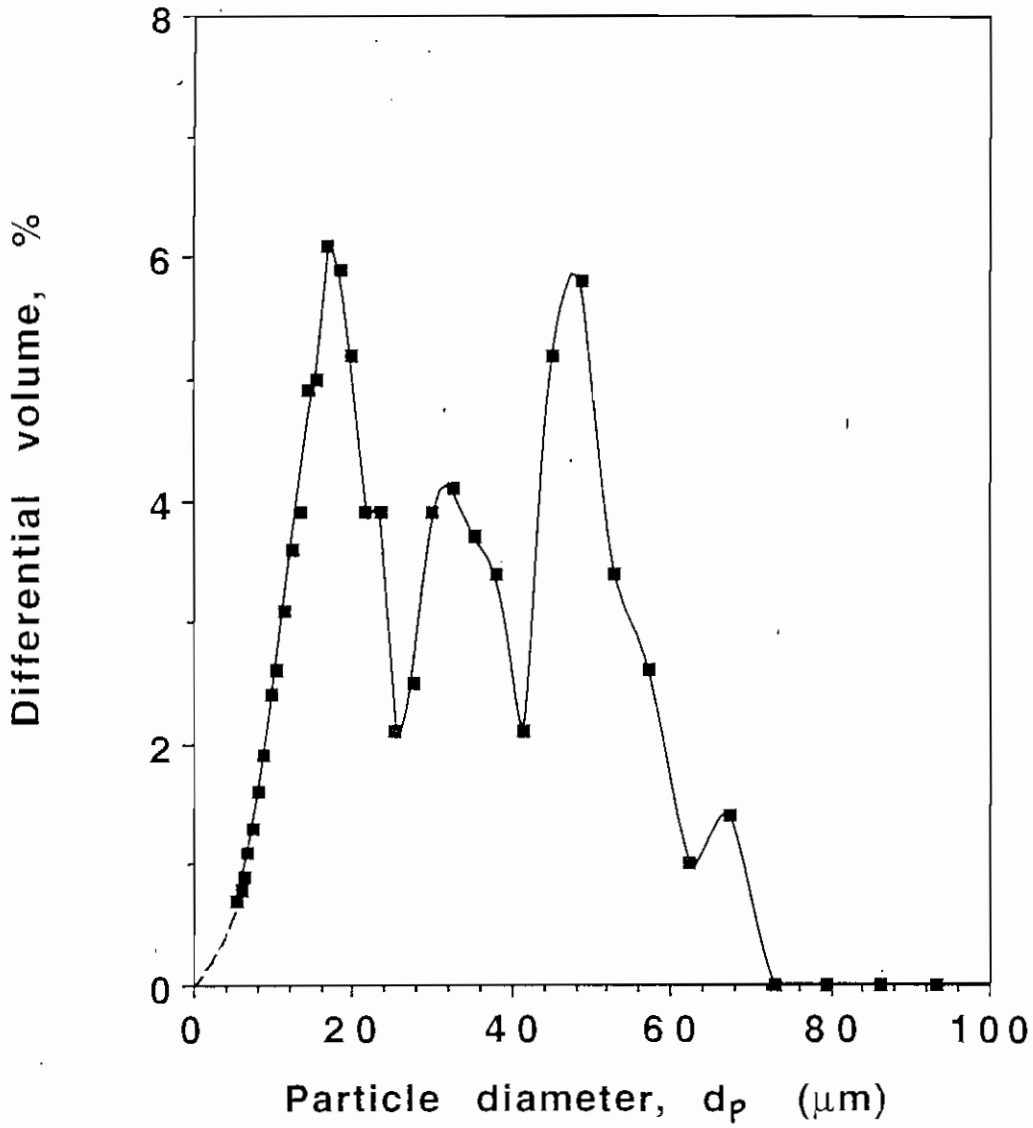

Fig. 1. Size distribution of suspended styrene-divinyl benzene particles.

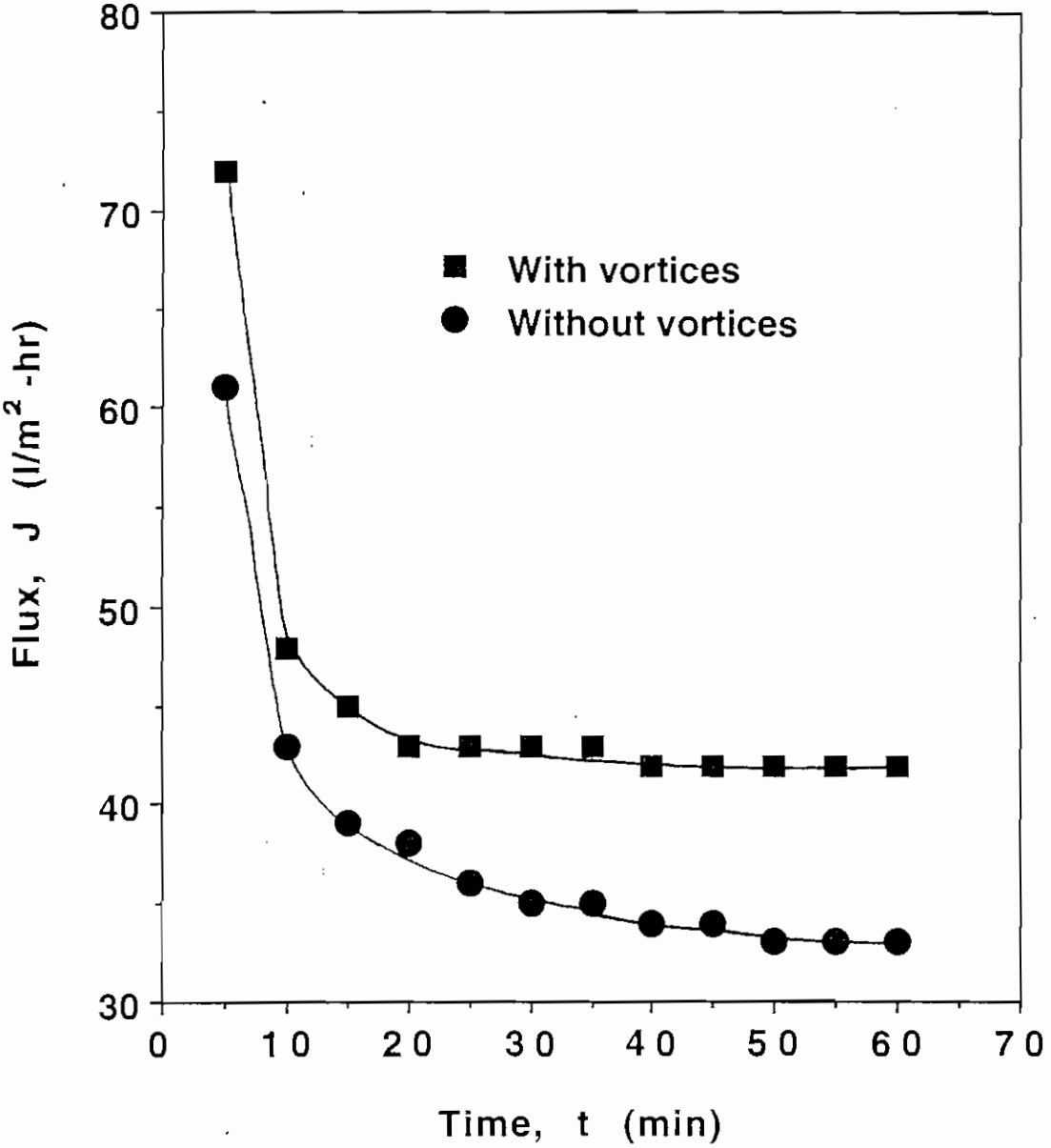

Fig. 2. Permeation flux characteristics of a 0.2 μm PSf membrane, at a 25 μm S/DVB particle suspension concentration of 0.15 wt % and a D = 4.77 (De_c = 35.71). ΔP = 69.8 kPa. Pure water flux = 220.72 l/m^2-hr. Cross-flow velocity, v = 0.5689 m/s.

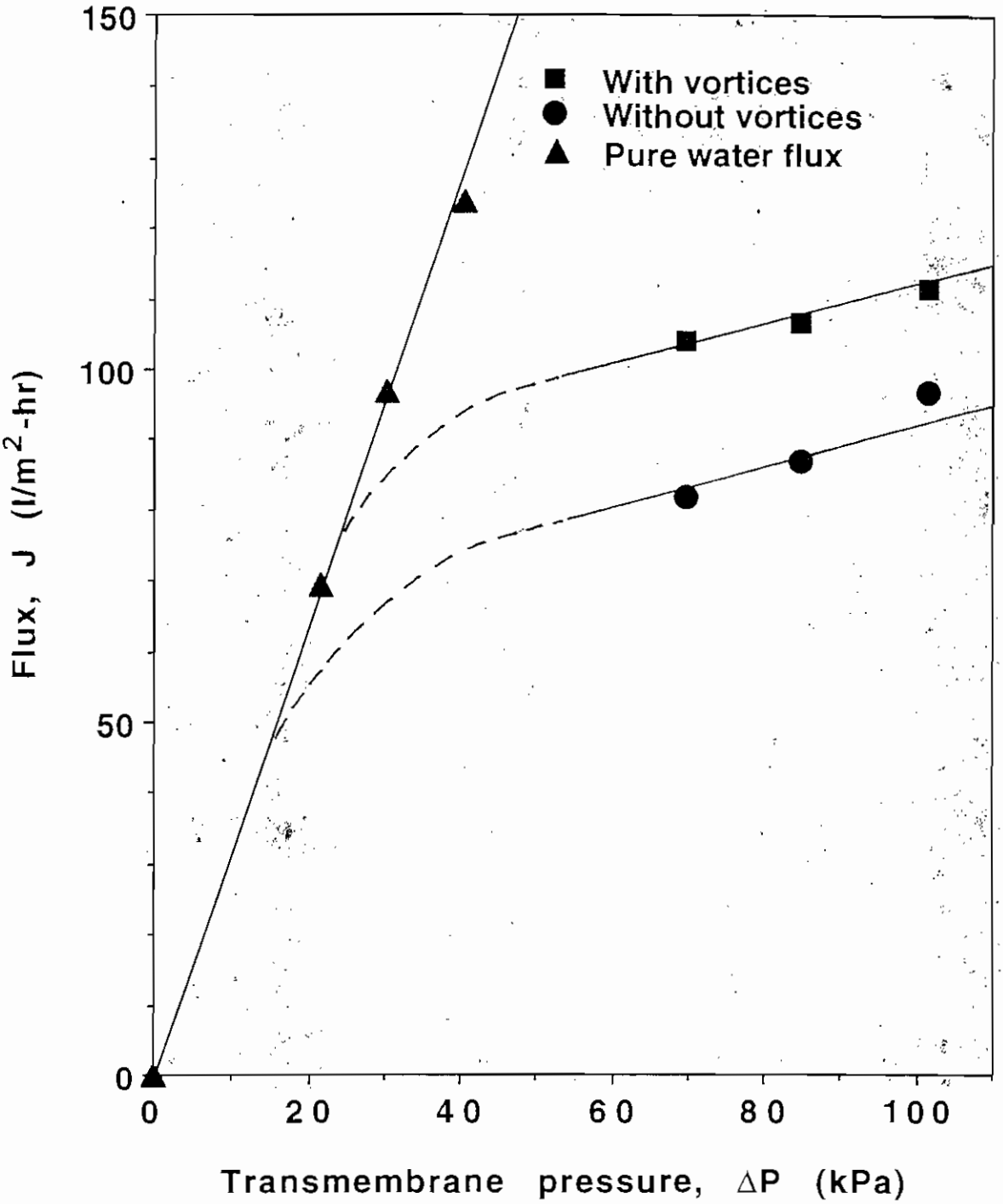

Fig. 3. Permeation flux characteristics of a 0.2 μm PSf membrane, at a 25 μm S/DVB particle suspension concentration of 0.15 wt % and a D = 4.77 (De_c = 35.71). Crossflow velocity, v = 0.5689 m/s.

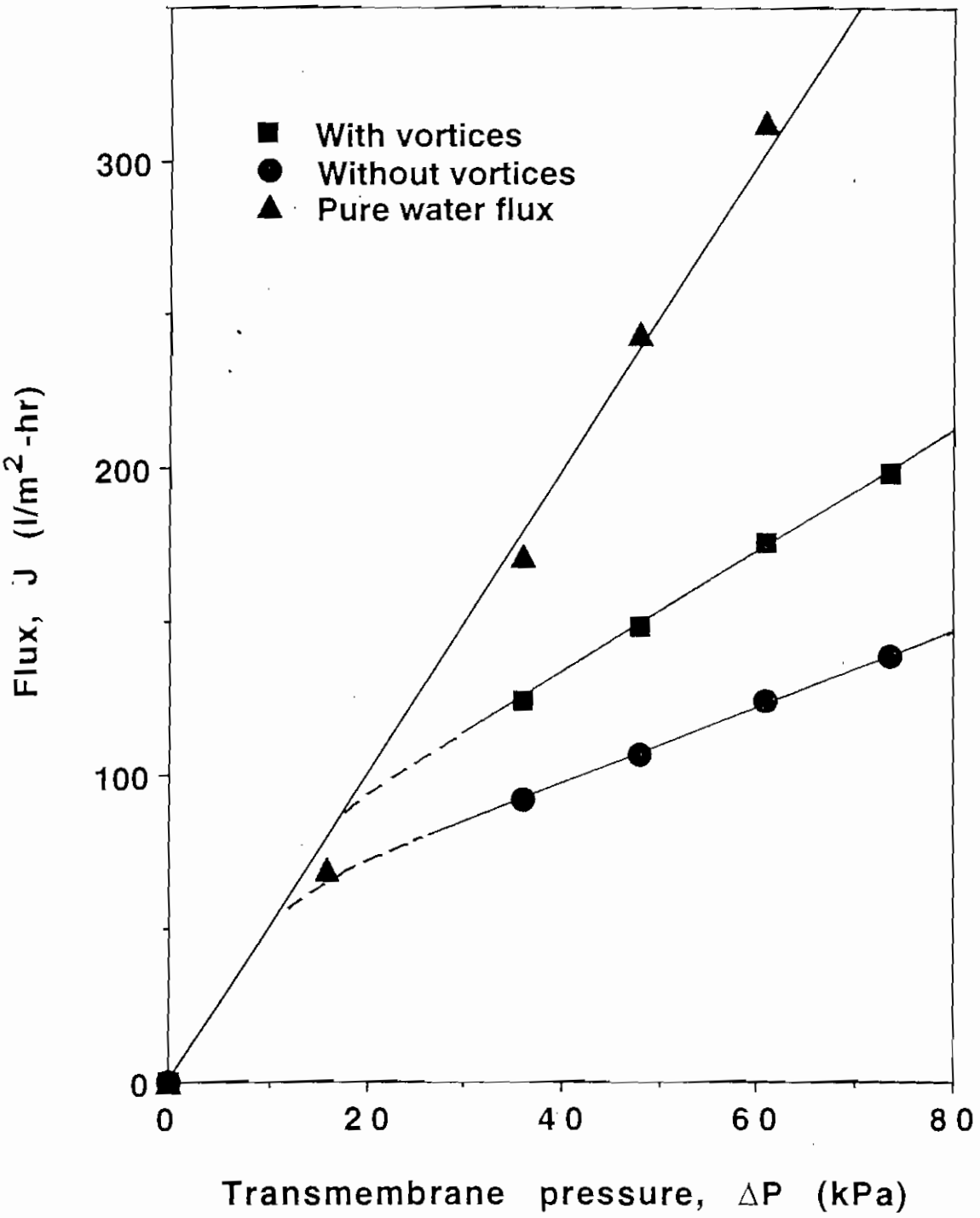

Fig. 4. Permeation flux characteristics of a 0.2 μm PP membrane, at a 25 μm S/DVB particle suspension concentration of 0.075 wt % and a D = 6.1 (De_c = 35.71). Cross-flow velocity, v = 0.7275 m/s.

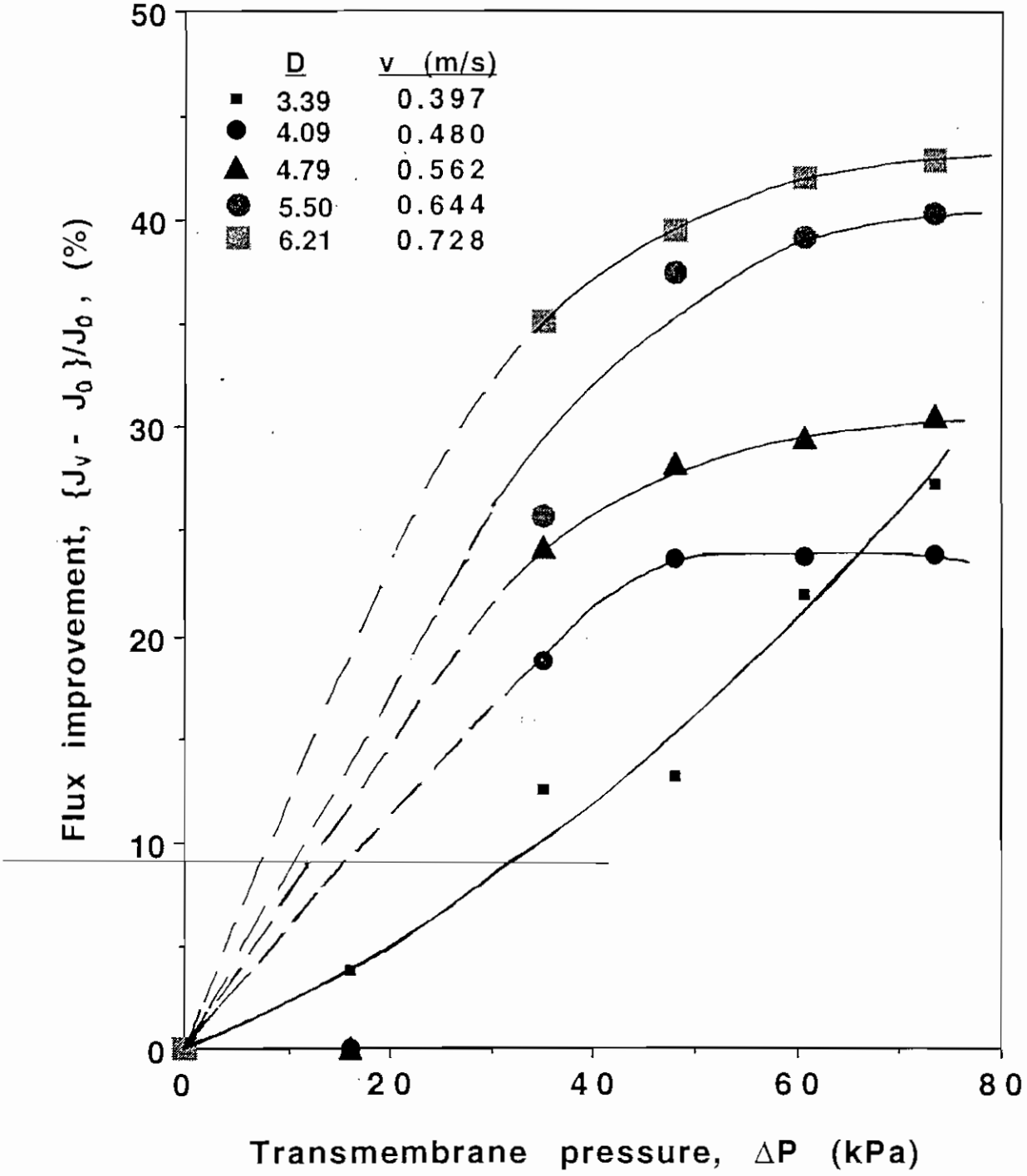

Fig. 5. Variation of flux enhancement with ΔP at a 25 μm S/DVB particle suspension concentration of 0.075 wt %, for a 0.2 μm PP membrane. J_v and J_0 are the permeation fluxes with and without vortices, respectively.

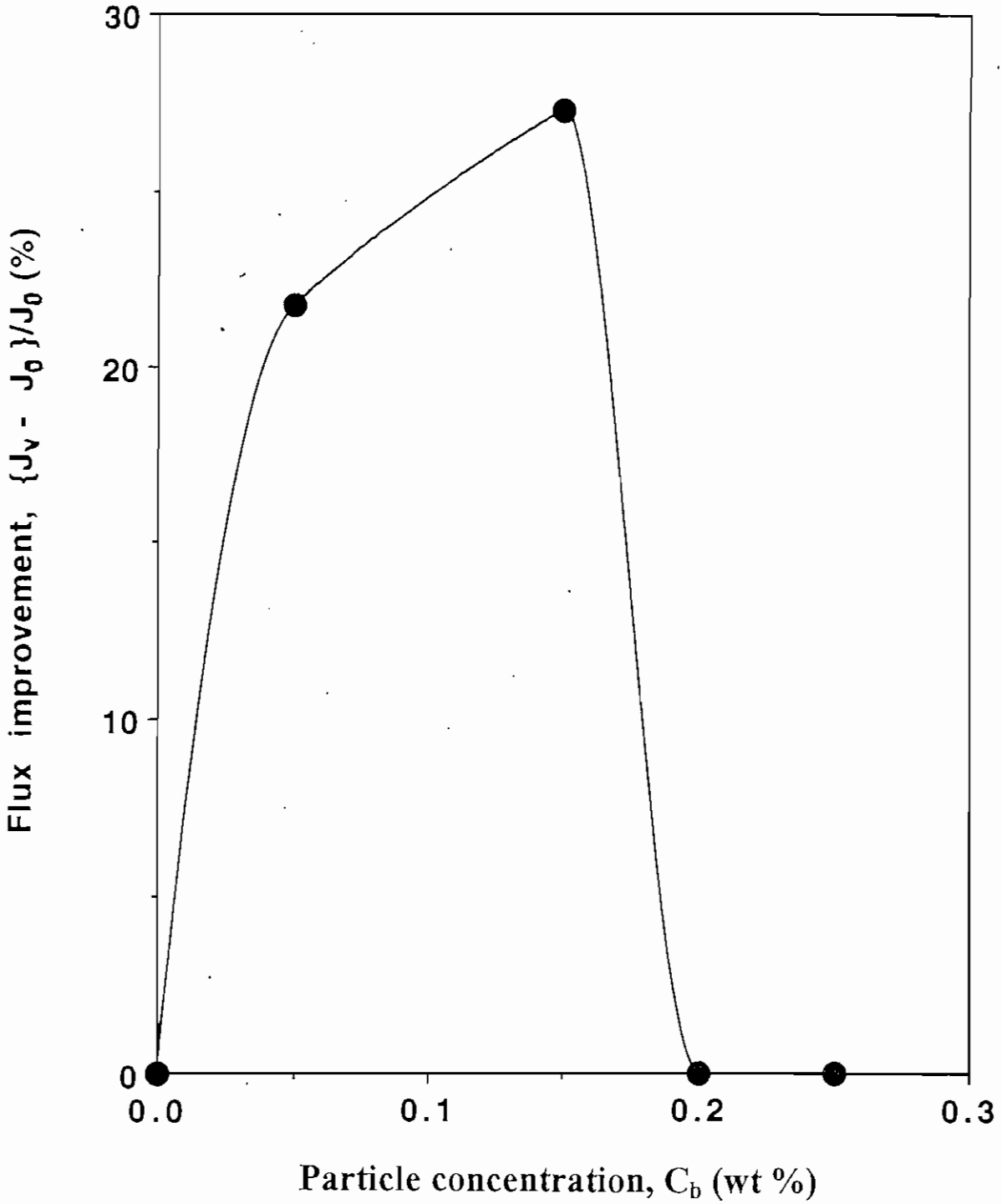

Fig. 6. Variation of flux enhancement with 25 μm S/DVB particle suspension concentration, at a D = 4.77 (De_c = 35.71) and ΔP = 69.8 kPa, for a 0.2 μm PSf membrane. Crossflow velocity, v = 0.5689 m/s.

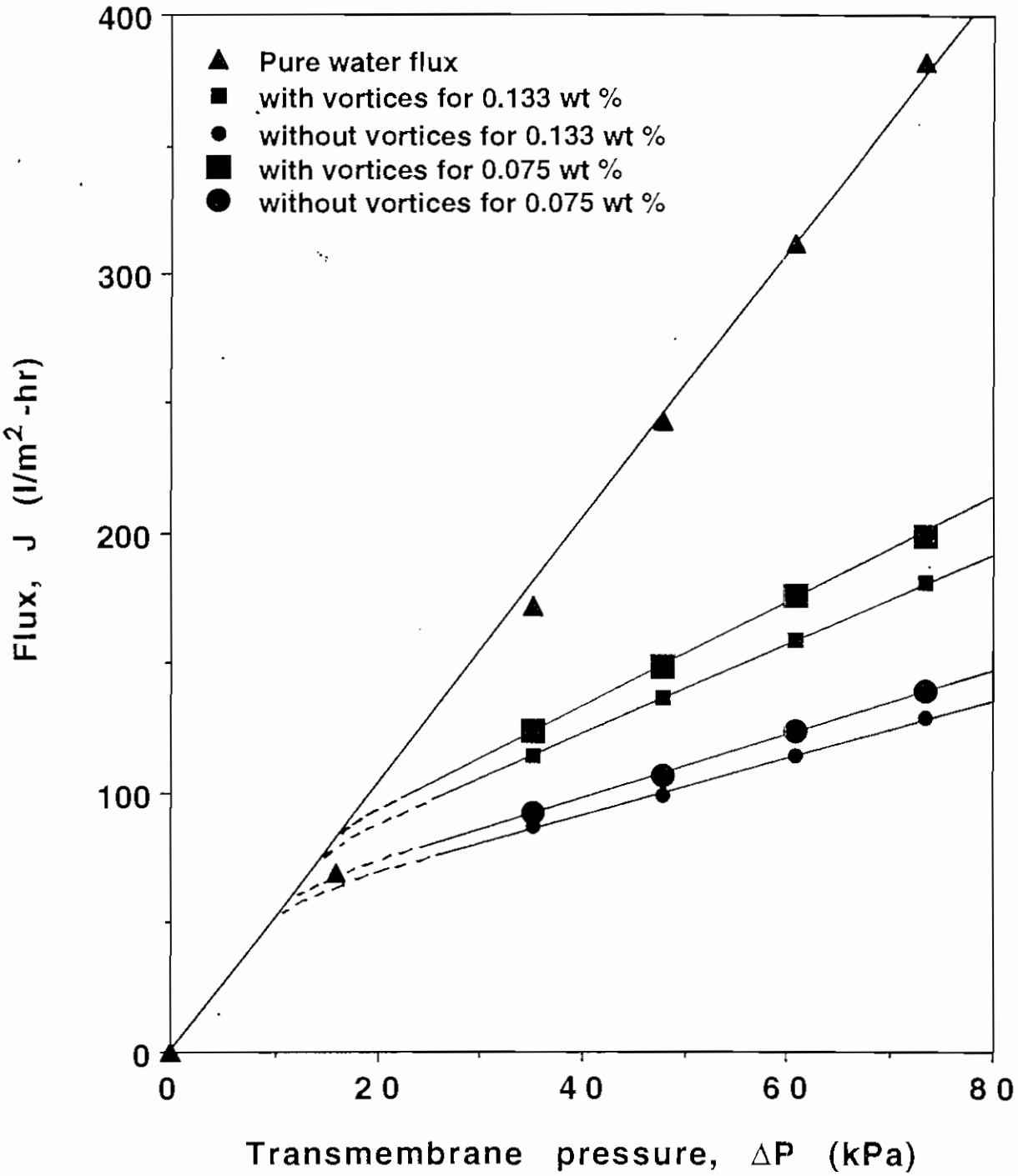

Fig. 7. Permeation flux characteristics of a 0.2 μm PP membrane, at a D = 6.1 (De_c = 35.71). Crossflow velocity, v = 0.7275 m/s.

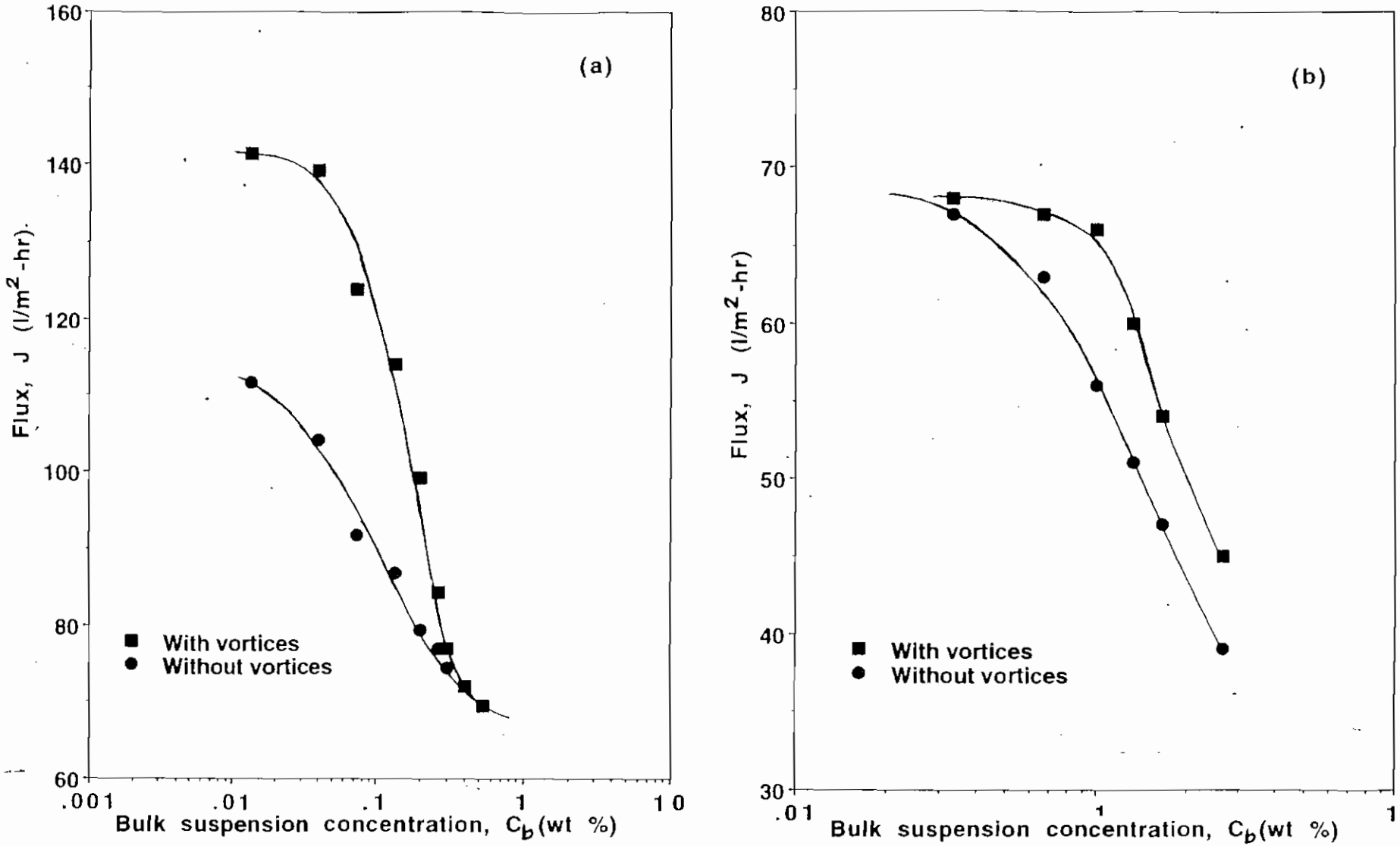

Fig. 8. Permeation flux versus logarithm of the bulk concentration for (a) 25 μm S/DVB and (b) 20 μm silica particle suspensions. ΔP = 35 kPa, D = 6.1 and 0.2 μm PP membrane.

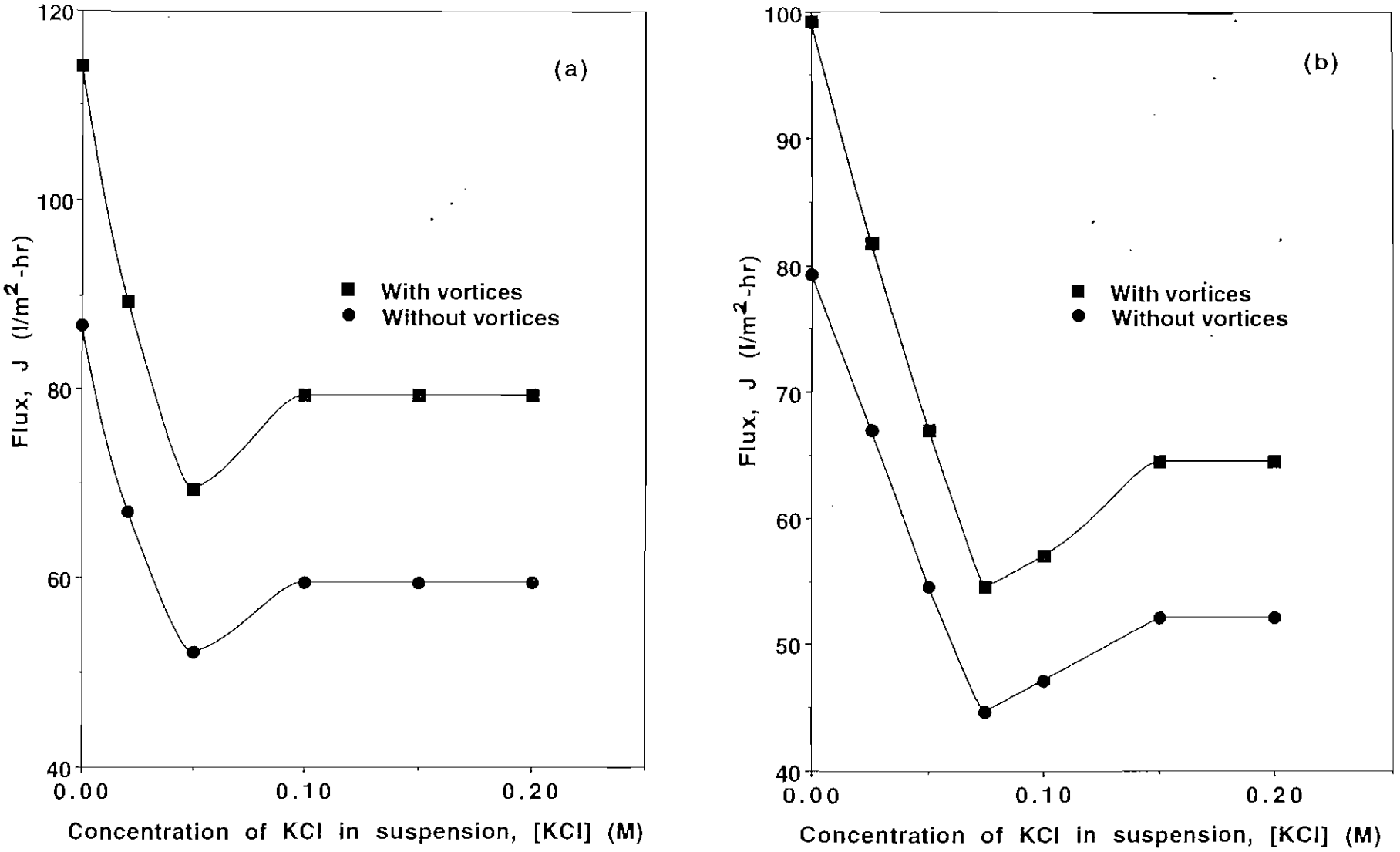

Fig. 9. Permeation flux as a function of KCl addition to a (a) 0.133 wt % and (b) 0.2 wt % 25 μm S/DVB particle suspension at ΔP = 35 kPa and D = 6.1. A 0.2 μm PP membrane was used.

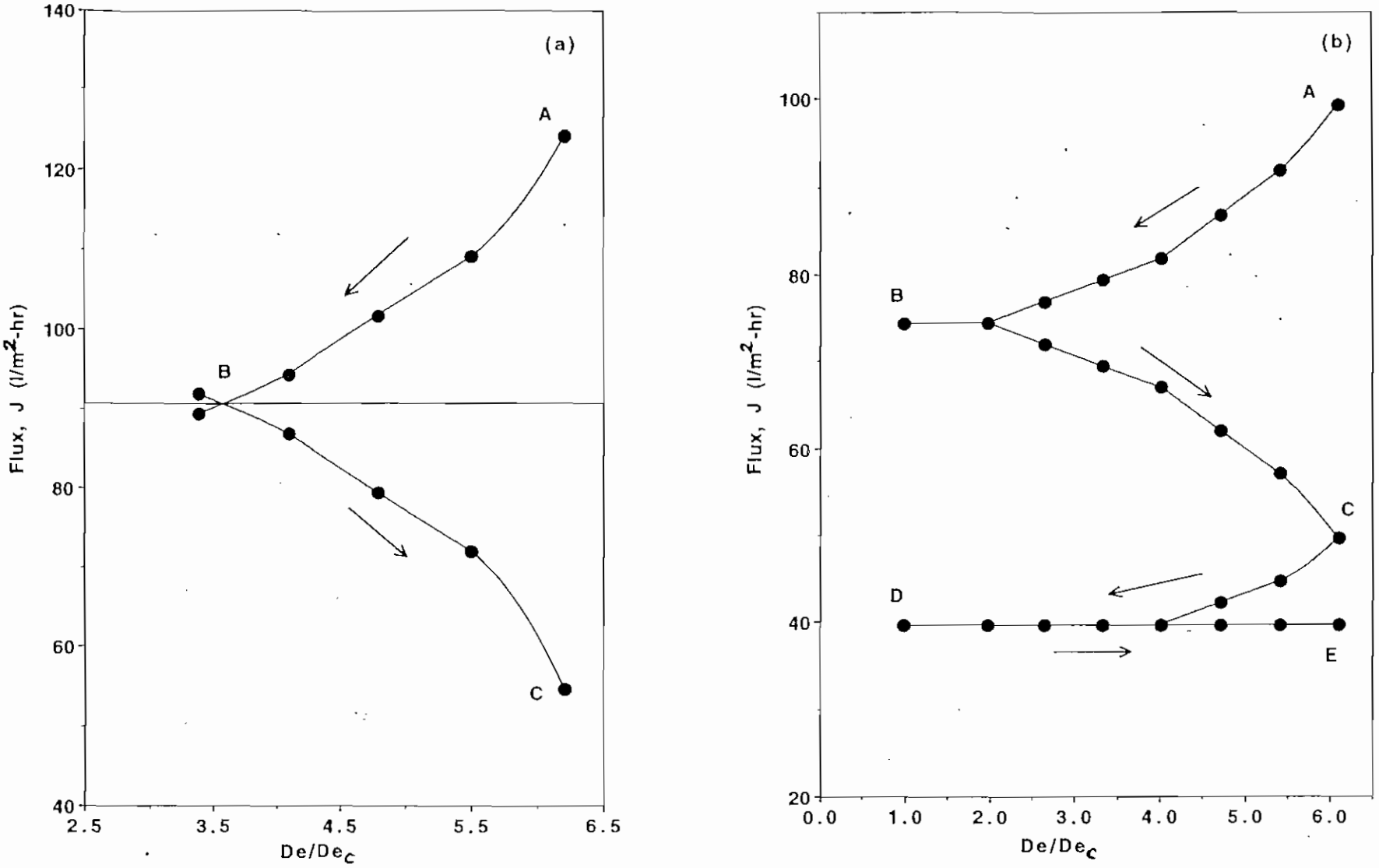

Fig. 10. Permeation flux as a function of decreasing and increasing flow rate (D), for (a) 0.075 wt % and (b) 0.2 wt % S/DVB particle suspension at 35 kPa and D = 0.98 to 6.1 (De = 35.71), the pure water flux was 175 l/m -hr. A 0.2 μm PP membrane was used.

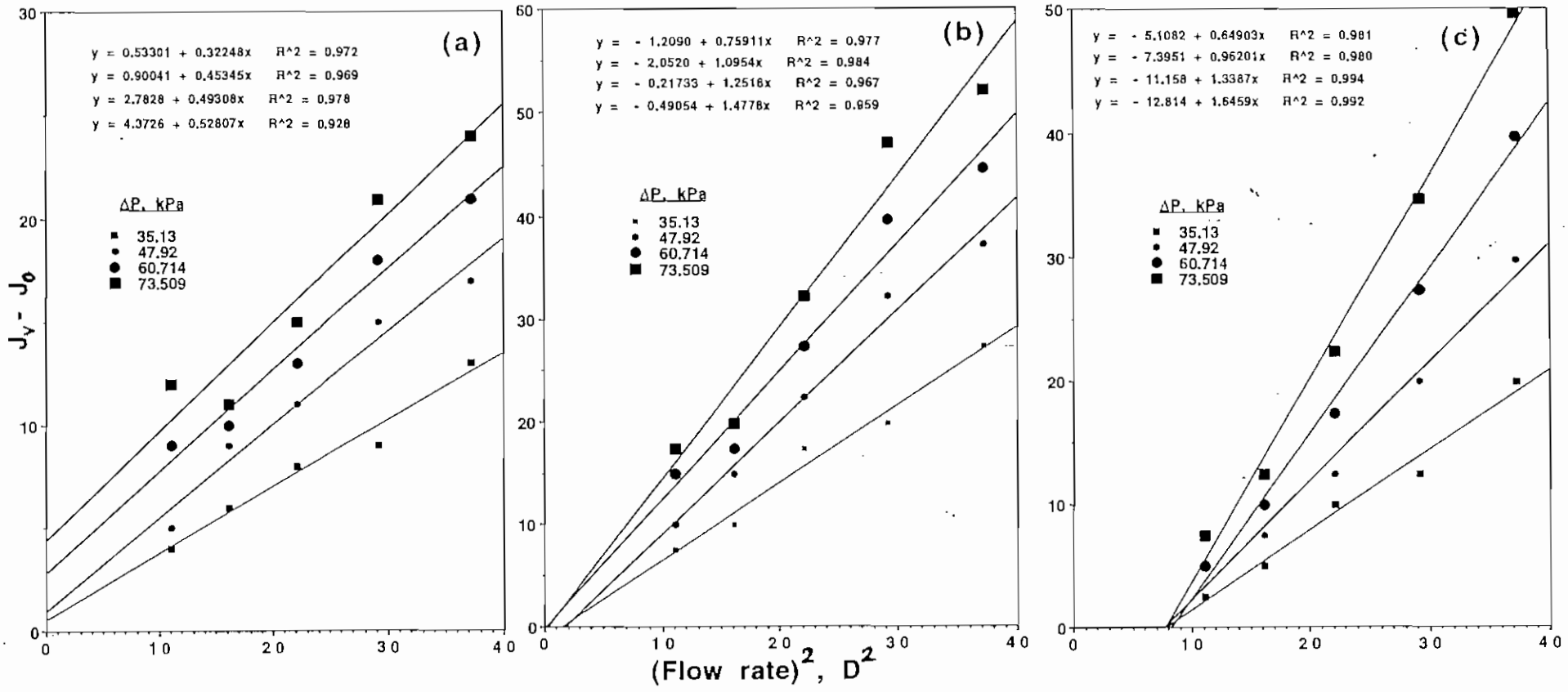

Fig. 11. Improved permeation flux as a result of increasing flow rate above D = 1, for different transmembrane pressures.
For (a) 0.075 wt %, (b) 0.133 wt % and (c) 0.2 wt %, 25 μm S/DVB particle concentration with a 0.2 μm PP membrane.

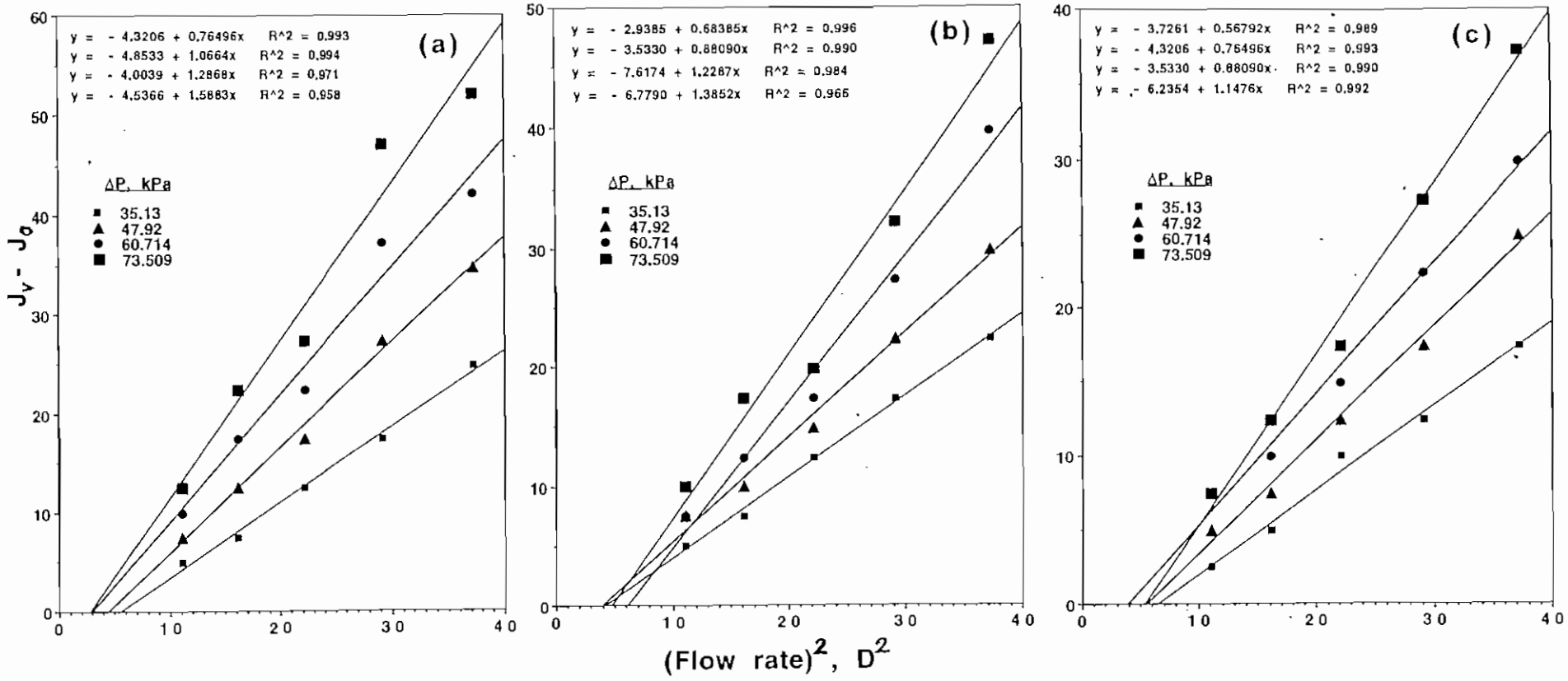

Fig. 12. Improved permeation flux as a result of increasing flow rate above D = 1, for different transmembrane pressures.
For (a) 0.1 wt %, (b) 0.133 wt %, and (c) 0.166 wt %, 20 μm silica particle concentration with a 0.2 μm PP membrane.

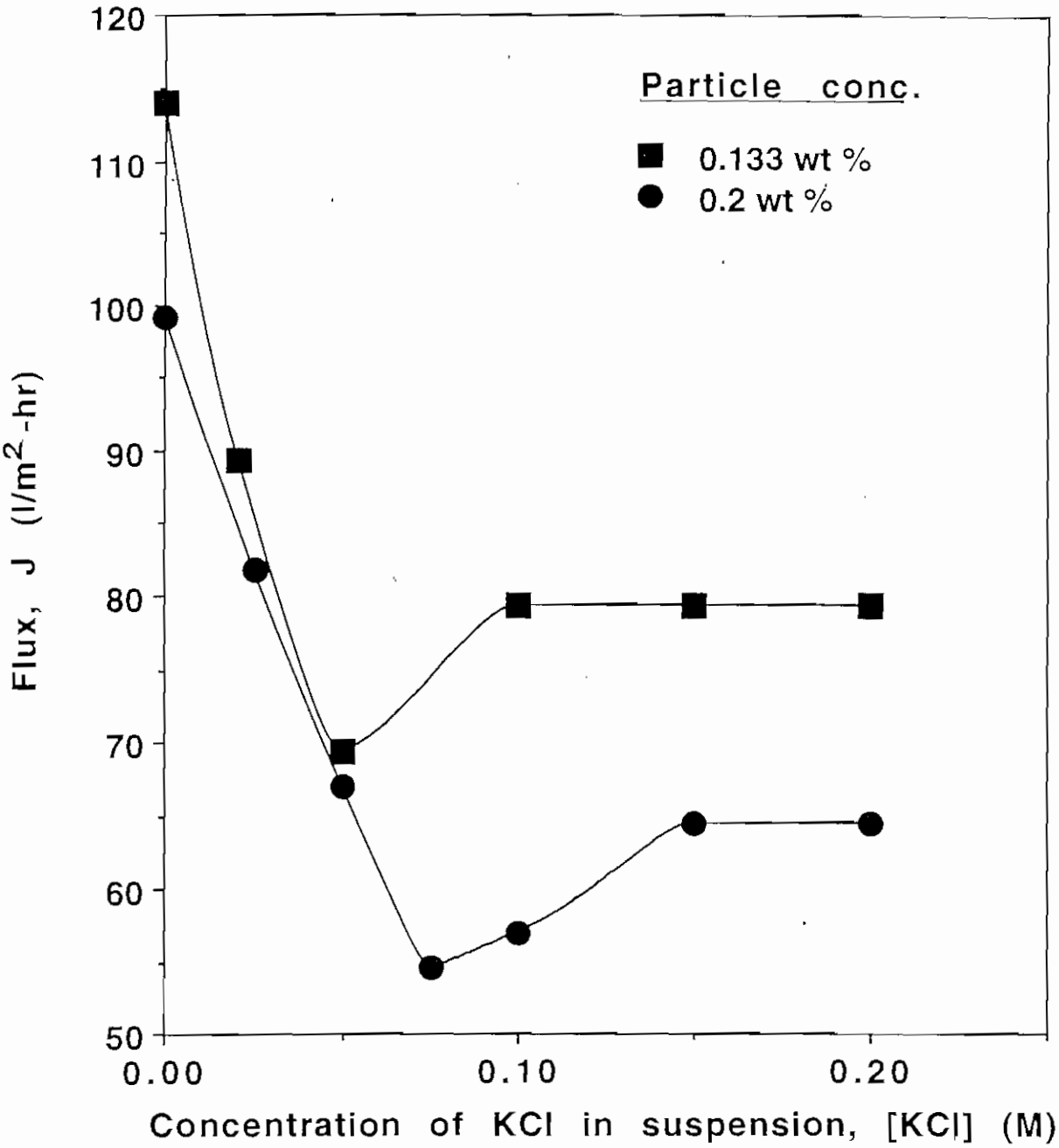

Fig. 13. Effect of salt concentration on flux in the presence of vortices for S/DVB particle suspensions at two concentrations. D = 6.1, ΔP = 35 kPa and 0.2 μm PP membrane.

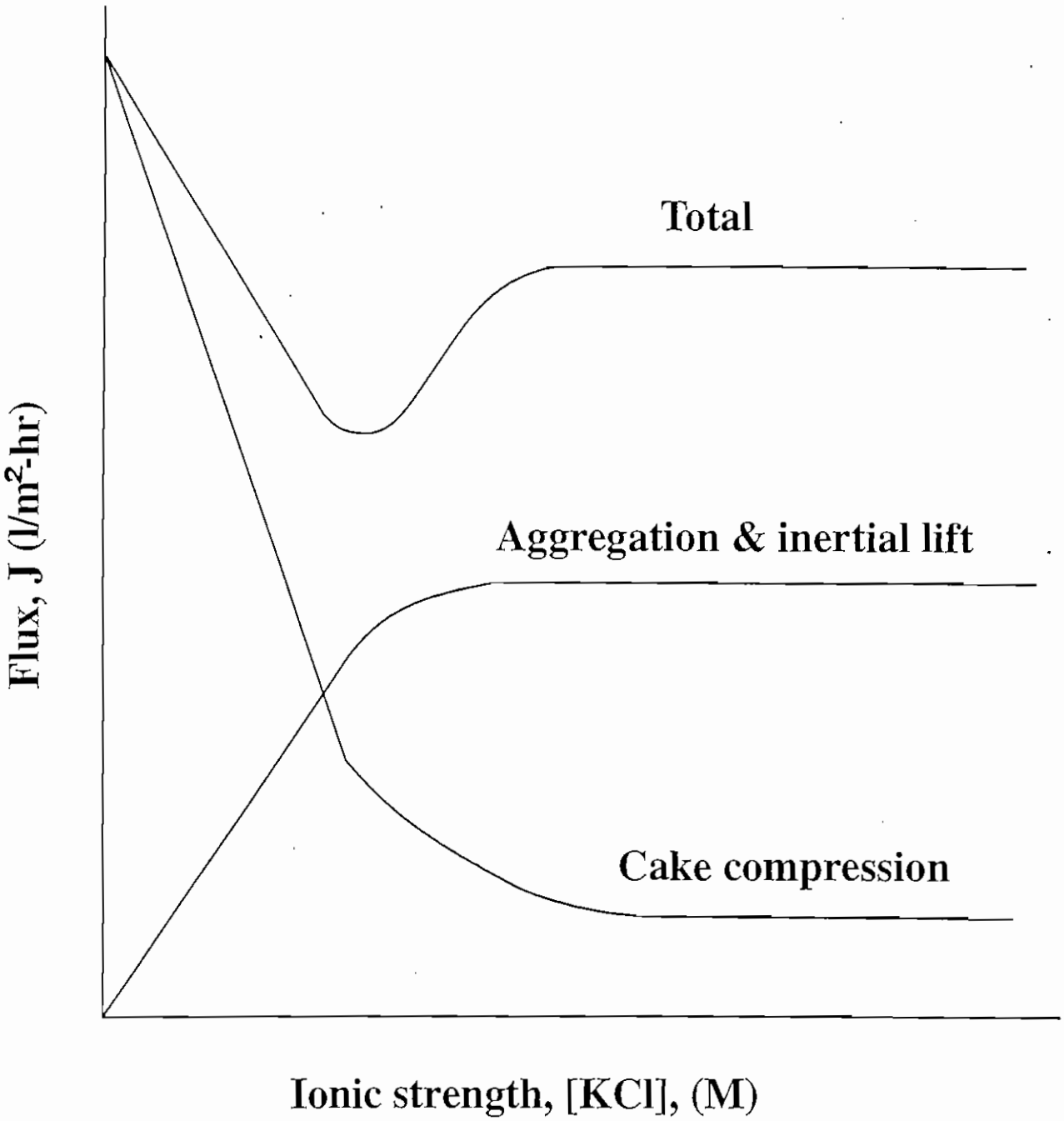

Fig. 14. Schematic showing two competing effects of (i) aggregation and inertial lift and (ii) cake compression resulting from salt addition.

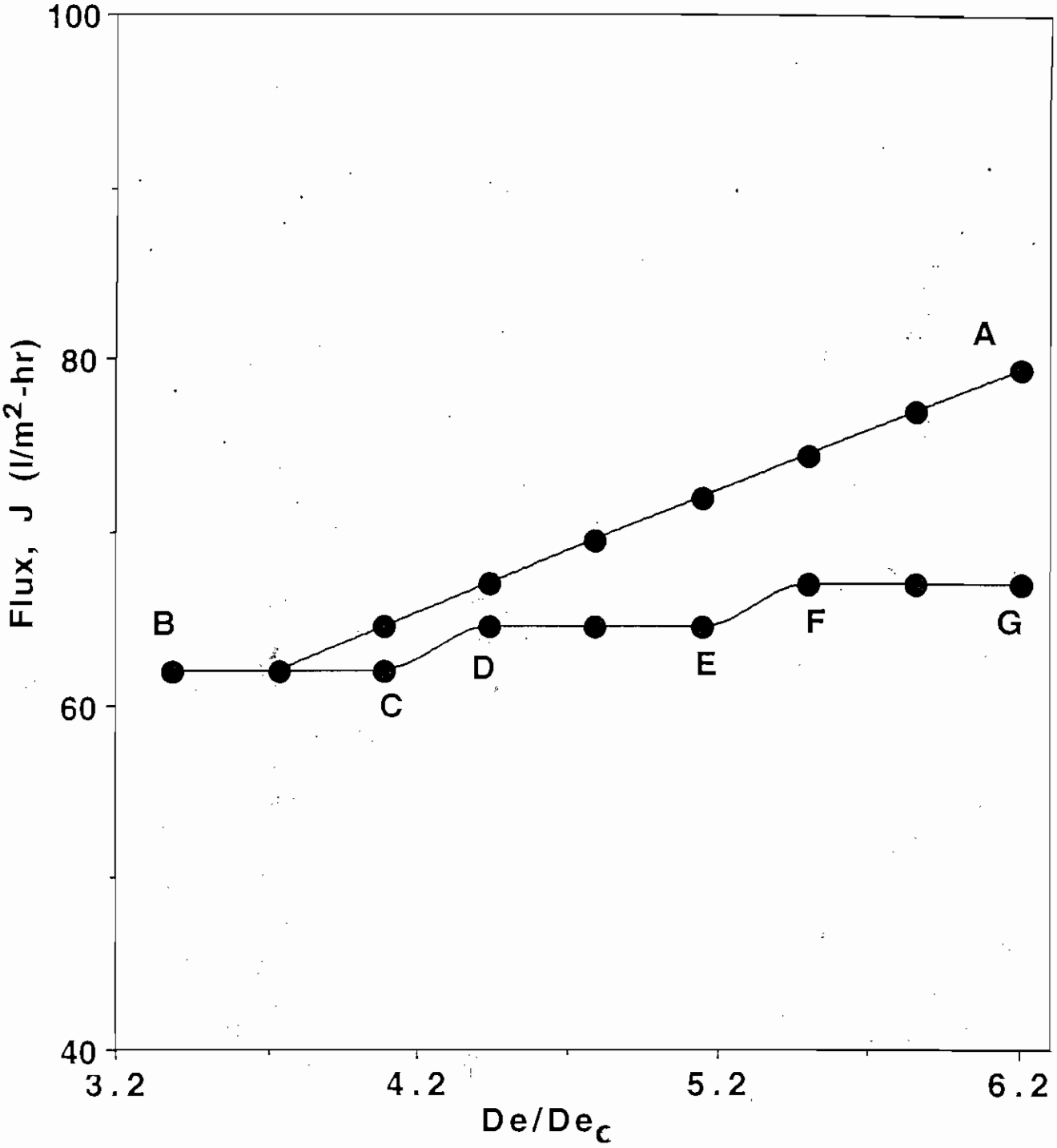

Fig. 15. Permeation flux as a function of decreasing and increasing flow rate (D), for a 0.133 wt % 25 μm S/DVB particle suspension at 35 kPa and 0.15 M KCl concentration with 0.2 μm PP membrane.

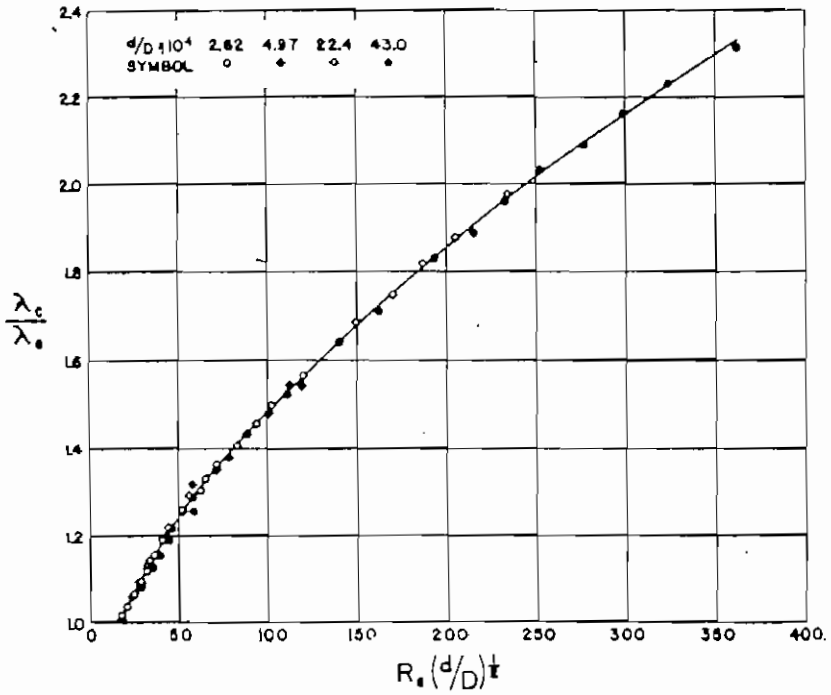

Fig. 16. Ratio of the bend coefficient, λ_c, to the straight pipe coefficient, λ_s, as a function of $Re(d/D)^{1/2}$ [34].